

Skillful Kilometer-Scale Regional Weather Forecasting via Global and Regional Coupling

WeiQi Chen
DAMO Academy, Alibaba Group
Hangzhou, China

Wenwei Wang
DAMO Academy, Alibaba Group
Hangzhou, China

Qilong Yuan
Northwest Polytechnical University
Xi'an, China

Lefei Shen
Zhejiang University
Hangzhou, China

Bingqing Peng
DAMO Academy, Alibaba Group
Hangzhou, China

Jiawei Chen
Zhejiang University
Hangzhou, China

Bo Wu
Institute of Atmospheric Physics,
Chinese Academy of Sciences
Beijing, China

Liang Sun
DAMO Academy, Alibaba Group
Hangzhou, China

Abstract

Data-driven weather models have advanced global medium-range forecasting, yet high-resolution regional prediction remains challenging due to unresolved multiscale interactions between large-scale dynamics and small-scale processes such as terrain-induced circulations and coastal effects. This paper presents a **global-regional coupling framework** for kilometer-scale regional weather forecasting that synergistically couples a pretrained Transformer-based global model with a high-resolution regional network via a novel bidirectional coupling module, **ScaleMixer**. ScaleMixer dynamically identifies meteorologically critical regions through adaptive key-position sampling and enables cross-scale feature interaction through dedicated attention mechanisms. The framework produces forecasts at 0.05° ($\sim 5\text{km}$) and 1-hour resolution over China, significantly outperforming operational NWP and AI baselines on both gridded reanalysis data and real-time weather station observations. It exhibits exceptional skill in capturing fine-grained phenomena such as orographic wind patterns and Foehn warming, demonstrating effective global-scale coherence with high-resolution fidelity. The code is available at <https://anonymous.4open.science/r/ScaleMixer-6B66>.

Keywords

Regional weather forecasting, Downscaling, Deep Neural networks

ACM Reference Format:

WeiQi Chen, Wenwei Wang, Qilong Yuan, Lefei Shen, Bingqing Peng, Jiawei Chen, Bo Wu, and Liang Sun. 2018. Skillful Kilometer-Scale Regional Weather Forecasting via Global and Regional Coupling. In . ACM, New York, NY, USA, 24 pages. <https://doi.org/XXXXXXXX.XXXXXXX>

Permission to make digital or hard copies of all or part of this work for personal or classroom use is granted without fee provided that copies are not made or distributed for profit or commercial advantage and that copies bear this notice and the full citation on the first page. Copyrights for components of this work owned by others than the author(s) must be honored. Abstracting with credit is permitted. To copy otherwise, or republish, to post on servers or to redistribute to lists, requires prior specific permission and/or a fee. Request permissions from permissions@acm.org.
Conference'17, Washington, DC, USA

© 2018 Copyright held by the owner/author(s). Publication rights licensed to ACM.
ACM ISBN 978-1-4503-XXXX-X/2018/06
<https://doi.org/XXXXXXXX.XXXXXXX>

1 Introduction

Accurate weather forecasting is essential for disaster mitigation, agriculture, transportation, and energy management [6]. Traditional numerical weather prediction (NWP) systems solve the governing equations of atmospheric dynamics involving mass continuity, momentum conservation, and thermodynamics, and parameterize subgrid-scale processes such as turbulence and cloud microphysics [3, 13]. Although NWP models provide physically consistent forecasts and remain operational standards, their computational demands and sensitivity to parameterization schemes limit the skill in resolving kilometer-scale weather phenomena governed by multiscale interactions.

Recent data-driven AI models, particularly Transformer-based architectures trained on global reanalysis data such as ERA5, have achieved remarkable success in medium-range forecasting at synoptic scales at resolution of 0.25° and coarser. However, high-resolution operational regional forecasting (e.g., 0.05° , or $\sim 5\text{km}$) remains a significant challenge. Kilometer-scale weather is governed by complex multiscale interactions: large-scale circulations modulate local processes such as topographic flows, coastal breezes, and convective systems, while fine-scale features also feedback to broader dynamics. A prime example is the Hengduan Mountains, where large-scale dynamics including the Indian Monsoon, East Asian Monsoon, and Tibetan Plateau climate, interact with extreme terrain gradients. These terrain gradients, which exceed 3,000 m within 100 km, drive localized wind accelerations, sharp temperature contrasts, and convective processes that are poorly captured by coarse global models or isolated regional models [30]. Such intricate multiscale interactions challenge conventional models, necessitating forecasting models that reconcile global-scale coherence with high-resolution fidelity.

Recent studies have begun to explore data-driven regional weather forecasting and downscaling, typically treating global forecasts as static inputs [20, 21, 23, 26, 31]. However, these decoupled methods neglect dynamic cross-scale interactions and suffer from temporal misalignment between low-frequency global forecasts (e.g., 6-hourly) and high-resolution regional observations (e.g., hourly). In summary, to make accurate high-resolution regional weather

forecasting requires addressing two key challenges: (1) *a mechanism to dynamically identify regions where cross-scale interactions are active*, and (2) *a bidirectional coupling framework that ensures spatial-temporal consistency across scales*.

To address the aforementioned challenges, we propose a novel **global–regional coupling framework** for high-resolution regional weather prediction. Our approach seamlessly integrates a pretrained global Transformer model, which provides synoptic-scale (large scale) context, with a regional refinement model operating at 0.05° resolution. Central to this architecture is **ScaleMixer**, a module that adaptively identifies key spatial regions exhibiting strong multiscale interactions and enable bidirectional feature encoding between global and regional tokens. This allows the model to prioritize meteorologically critical areas such as typhoon boundaries and mountain ridges, and maintain global coherence while resolving fine-grained regional dynamics. The main contributions of this work are summarized as follows:

- A **global–regional coupling framework for 0.05° and 1-hour forecasting** by integrating a pretrained global model for synoptic-scale context with a high-resolution regional model
- The **ScaleMixer** module for dynamic identification of cross-scale interaction regions and bidirectional feature fusion.
- Experiments on both hindcast and operational settings show our model’s superiority against operational NWP and leading AI baselines. Case studies over complex terrain in China further demonstrates the model’s notable skill in capturing orographic wind effects and Foehn warming.
- Similar to other AI-based models, the model is highly efficient during inference. It takes less than 3 minutes for 48-hour forecasting on a single GPU, while numerical models like IFS-HRES typically requires about 1 hour on massive CPU clusters for a similar forecasting window.

2 Related Work

Numerical Weather Forecasting. As the predominant paradigm, NWP systems typically formulate the atmospheric physical laws through PDEs and then solve them using numerical simulations. Representative examples include earth system models (ESMs) [13] and the operational Integrated Forecast System (IFS) of European Centre for Medium-Range Weather Forecasts (ECMWF) [3]. By integrating physics laws, NWP approaches have enjoyed remarkable success with great accuracy, stability, and interpretability. IFS-HRES [10] is a world-leading high-resolution deterministic NWP system (0.1°) and serves as a benchmark for operational forecasting and research. However, NWP models are sensitive to initial conditions, prone to errors in parameterization, and computationally expensive [15]. These limitations hinder their ability to accurately resolve kilometer-scale weather driven by complex multiscale interactions.

Deep Learning for Global Weather Forecasting. Recent progress in deep learning models for global weather forecasting has been transformative. They predominantly employ two architectural paradigms:

Transformer-based models [2, 4, 5, 22] and Graph Neural Network (GNN)-based architectures [14, 16, 25]. These models demonstrate computational efficiency and competitive skill in predicting synoptic-scale weather patterns. However, they fail to capture finer-grained mesoscale weather dynamics due to limited resolution (0.25° or coarser).

Deep Learning for Regional Weather Forecasting and Downscaling. Recently, regional weather models have been developed for fine-scale forecasting and downscaling over regions of interest. For instance, CorrDiff [20] combines U-Net and diffusion models to correct and downscale the global forecasts to improve local predictions. Machine learning limited area models [1] further take into account boundary conditions, because the evolution of atmospheric states relies on both the internal dynamics and the external forcing. A sequence of GNN layers is applied to capture both large-scale circulations and local microscale processes. Other limited area modeling methods also employ GNN architectures with stretched-grid [11] and nested-grid [21] to make low-resolution global and high-resolution regional weather forecasts simultaneously. They model cross-scale interactions through grid deformation and nesting, with a static graph structure; however, these rigid, geometry-driven interactions limit the model’s ability to efficiently capture highly dynamic and non-local coupling processes. In contrast, our model employs a bidirectional coupling module to learn the content-dependent cross-scale interactions between global and regional tokens adaptively.

3 Methodology

Accurate regional weather forecasting requires seamless integration of large-scale atmospheric dynamics with localized, high-resolution features. As nearly all AI-based global models are trained on the EAR5 dataset, we assume a pretrained Vision Transformer (ViT)-based global weather forecasting model, denoted $\mathcal{M}_{\text{global}}$, which operates on low-resolution (0.25°) global reanalysis data $\mathbf{U}^{t_0} \in \mathbb{R}^{H \times W \times C}$. At time t_0 , the model generates 6-hour-ahead global predictions capturing synoptic-scale dynamics:

$$\hat{\mathbf{U}}^{t_0+6H} = \mathcal{M}_{\text{global}}(\mathbf{U}^{t_0}), \quad (1)$$

where $H \times W \times C$ represents the stacked weather state with multiple levels of upper air and surface variables, in which latitude and longitude are divided into H and W grids for each variable. Concurrently, high-resolution regional analysis data $\mathbf{u}^{t_0} \in \mathbb{R}^{h \times w \times V_{\text{reg}}}$ provides critical surface variables (wind components U, V , temperature T , specific humidity Q , pressure P , radiation fluxes $SSRD$, and total cloud cover TCC) within a region of interest at 1 hour temporal resolution and 0.05° spatial resolution.

Problem Formulation. As the fundamental challenge lies in effectively coupling multiscale information: coarse-grained global features from $\mathcal{M}_{\text{global}}$ and fine-resolution regional features, we formalize the task as developing a hybrid global-regional weather forecasting framework $\mathcal{M}_{\text{global-regional}}$ that extends $\mathcal{M}_{\text{global}}$ through the integration of large-scale atmospheric dynamics and small-scale weather effects.

$$\hat{\mathbf{U}}^{t_0+6H}; \{\hat{\mathbf{u}}^{t_0+iH}\}_{i=1}^6 = \mathcal{M}_{\text{global-regional}}\left(\mathbf{U}^{t_0}; \{\mathbf{u}^{t_0+iH}\}_{i=-5}^0\right), \quad (2)$$

where $\{\hat{\mathbf{u}}^{t_0+iH}\}_{i=-5}^0$ denotes the temporally aligned regional analysis data with 1-hour intervals. This formulation establishes a principled framework for generating high-fidelity regional forecasts by systematically bridging global-scale dynamics with localized meteorological processes with deep learning architectures.

Model Overview. We propose a multiscale weather forecasting framework that dynamically integrates global and regional-scale atmospheric dynamics to resolve high-resolution mesoscale features in the target region. As shown in Figure 1, the framework comprises two Transformer-based sub-models with shared architectural principles: (1) a global model for synoptic-scale dynamics, and (2) a regional model for mesoscale processes. The ScaleMixer module enables bidirectional coupling between the global and regional models via adaptive key position identification and encoding to preserve cross-scale meteorological consistency. The global model, pretrained on ERA5 reanalysis data [12], remains fixed during regional optimization, while the regional model and ScaleMixer module are trained from scratch.

3.1 Pretrained Global Weather Model

Our global model $\mathcal{M}_{\text{global}}$ prioritizes architectural simplicity, flexibility, and scalability, and implements a vision Transformer (ViT) architecture [7]. Without loss of generality, our framework can work with any ViT-based global weather forecasting model. In the following discussion, we will limit the discussion on our in-house developed ViT-based global model, comprising three core components:

Patch Embedding and Tokenization: A 2-D convolutional layer partitions the multivariate input atmospheric state $\mathbf{U}^{t_0} \in \mathbb{R}^{H \times W \times C}$ into non-overlapping spatial patches of size $P \times P$. This generates token representations $\mathbf{S} \in \mathbb{R}^{N \times d}$, where $N = (H/P) \times (W/P)$ and d is the embedding dimension.

Transformer Encoder: A stack of M Transformer encoder layers processes the sequence \mathbf{S} through multi-head self-attention and feed-forward networks [7, 29], enabling global information interaction across spatial scales.

Prediction Head: A deconvolution block upscales the processed sequence back to the original spatial resolution $H \times W$, producing a 6-hour ahead deterministic global forecast \mathbf{U}^{t_0+6H} of the full atmospheric state.

The global model $\mathcal{M}_{\text{global}}$ is pretrained on ERA5 reanalysis [12] using weighed mean absolute error (MAE) as the loss function (detailed in Section 3.4). The dataset includes five pressure level variables (13 vertical levels each): geopotential (z), specific humidity (q), wind components (u, v), and temperature (t), and multiple surface variables, e.g., 2-meter temperature ($t2m$), 10-meter wind ($u10, v10$), and mean sea level pressure (msl), surface pressure (sp), etc. (detailed in Section B).

3.2 Modifications in Regional Weather Model

The regional model $\mathcal{M}_{\text{regional}}$ inherits the Transformer architecture from the global model but introduces necessary modifications: (1) modified patch embedding layer to incorporate fine-grained topography and temporal encodings, (2) enhanced prediction head with adaptive layer normalization (AdaLN) [24] to amplify the high-frequency signal for hourly temporal alignment, and (3) fewer

Transformer encoder layers ($k \ll M$) to reduce computational overhead while preserving regional meteorological fidelity.

Patch Embedding: In addition to the input $\{\mathbf{u}^{t_0+iH}\}_{i=-5}^0 \in \mathbb{R}^{h \times w \times V_{\text{reg}} \times 6}$, the block also needs to process the static topography, land-sea mask, and dynamic hourly temporal information. Regional analyses are tokenized across 6 time steps using a shared patch embedding layer, with topography, land-sea masks, and temporal embeddings (hour-of-day, day-of-year) added via MLP. To ensure geographic consistency with global patches, we set patch size $p = 5 \times P$, generating regional tokens $\mathbf{s} \in \mathbb{R}^{n \times d}$, where $n = (h/p) \times (w/p)$.

Transformer Encoders: The regional model employs k encoder layers ($k \ll M$, where $M = k \times L$) to achieve computational efficiency in regional optimization. Each cross-scale coupling block comprises L global encoder layers, 1 regional encoder layer, and 1 ScaleMixer module.

Prediction Head: To generate 6-hour forecasts at hourly intervals, 6 dedicated prediction heads produce lead time-specific outputs ($\Delta t = 1H$ to $6H$). Temporal alignment is enforced via AdaLN[24], where scale and shift parameters γ, β are derived from Fourier embeddings of Δt :

$$\text{FourierEmbed}(\Delta t) = [\cos(2\pi a_i \Delta t + b_i), \sin(2\pi a_i \Delta t + b_i)] \quad (3)$$

for $0 \leq i < d/2$,

$$\gamma, \beta = \text{MLP}(\text{FourierEmbed}(\Delta t)), \quad (4)$$

where a_i and b_i are learnable Fourier embedding parameters. This formulation ensures high-frequency signal amplification for regional forecasting. Moreover, regional prediction heads take the concatenation of regional tokens and spatially-aligned global tokens as input to make full use of multi-scale information.

3.3 ScaleMixer: Bidirectional Global and Regional Scale Coupling

Accurate high-resolution regional prediction requires resolving multiscale atmospheric processes—from synoptic-scale forcings to mesoscale circulations—while maintaining global dynamical consistency. To this end, we introduce **ScaleMixer**, a differentiable coupling mechanism that explicitly models interactions between the global foundation model and the regional refinement model. As illustrated in Figure 1 (right), ScaleMixer enables bidirectional feature fusion by adaptively identifying meteorologically critical regions and performing token-level encoding, effectively prioritizing areas with strong cross-scale interactions.

Adaptive key position identification. To capture spatial regions exhibiting strong multiscale interactions, we implement a dynamics-aware sampling module that identifies critical spatial positions from global token embeddings \mathbf{S} . Spatial dynamics are extracted via a convolutional network, followed by softmax-normalized importance scores $\text{Pr} \in \mathbb{R}^N$ (N is the number of global tokens):

$$\text{Pr} = \text{Softmax}(\text{Conv}(\mathbf{S})), \quad (5)$$

where $\text{Conv}(\cdot)$ consists of a convolutional layer followed by a linear projection. We then select top- m salient positions:

$$\mathbf{c} = \arg \text{top-}m(\text{Pr}), \quad \mathbf{h} = \text{Pr}[\mathbf{c}] \odot \mathbf{S}[\mathbf{c}], \quad (6)$$

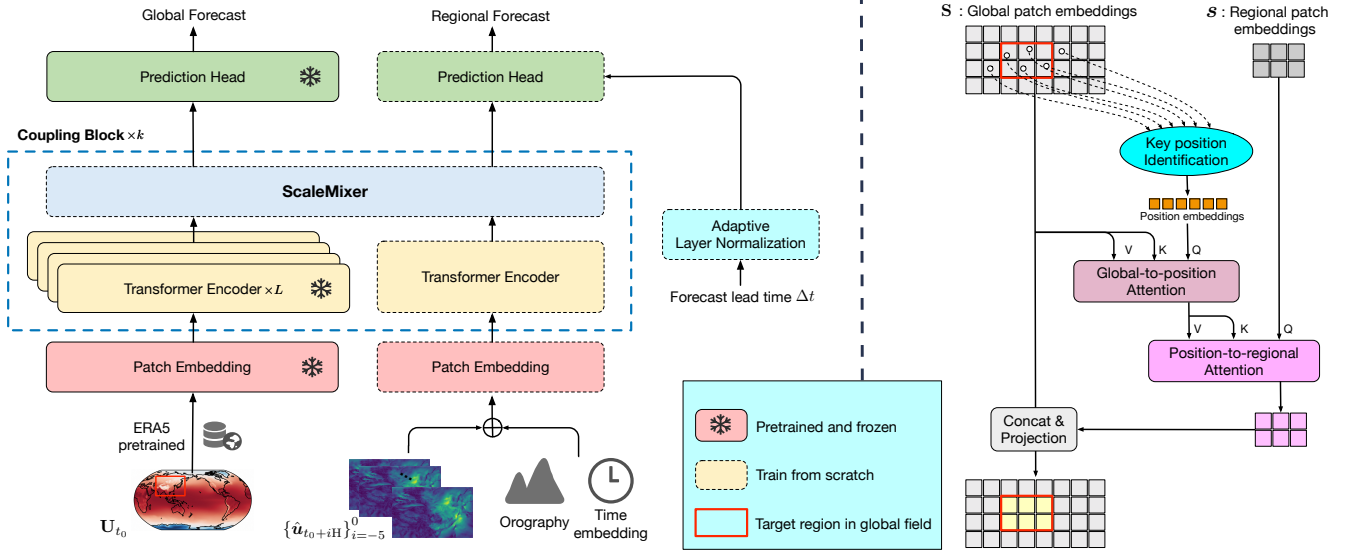


Figure 1: Left: The Architecture of Global-Regional Weather Forecasting Model: Synoptic-scale context ($\mathcal{M}_{\text{global}}$) drives mesoscale regional refinement ($\mathcal{M}_{\text{regional}}$) via ScaleMixer, ensuring cross-scale coupling and consistency. Right: ScaleMixer Module: Bidirectional Cross-Scale Coupling via Key Position Identification and encoding. Key components include (1) key position identification, (2) coupling regional dynamics with global context via global-to-position and position-to-regional attention, and (3) global token adaptation incorporating regional features.

with \odot denoting element-wise product, $\mathbf{c} = \{\mathbf{c}_i\}_{i=1}^m \in \mathbb{R}^{m \times 2}$ ($\mathbf{p}_i \in [0 : H/P - 1] \times [0 : W/P - 1]$) representing the coordinates of m selected tokens, and $\mathbf{h} \in \mathbb{R}^{m \times d}$ their corresponding embeddings.

Regional features alignment with global context. To effectively bridge the scale gap between global context and regional features, we design a two-stage cross-attention mechanism operating on identified key positions. Directly correlating all global and regional tokens is computationally expensive and may weaken localized meteorological features. Instead, we first condense global information into a sparse set of dynamically identified key positions, then propagate these enriched features to regional tokens.

Global-to-Position Attention first aggregates global context into the key positions. Using the concatenated token embeddings and coordinates of key positions $\mathbf{h}||\mathbf{c} \in \mathbb{R}^{m \times (d+2)}$ as queries, and the global tokens \mathbf{S} as keys and values, we compute:

$$\text{Glo-to-Pos}(\mathbf{h}||\mathbf{c}, \mathbf{S}, \mathbf{S}) = \text{Softmax} \left(\frac{(\mathbf{W}_Q \cdot \mathbf{h}||\mathbf{c})(\mathbf{W}_K \mathbf{S})^\top}{\sqrt{d}} \right) \mathbf{W}_V \mathbf{S}, \quad (7)$$

$$\mathbf{h}_{\text{global}}||\mathbf{c}' = \mathbf{h}||\mathbf{c} + \text{Glo-to-Pos}(\mathbf{h}||\mathbf{c}, \mathbf{S}, \mathbf{S}), \quad (8)$$

where \mathbf{W}_Q , \mathbf{W}_K and \mathbf{W}_V are linear projections. To better model the dynamics of key positions, the key representations are further refined by incorporating regional features via bilinear interpolation at the updated coordinates \mathbf{c}'

$$\mathbf{h}' = \text{MLP}_{\text{Proj}}(\text{Bilinear}(\mathbf{s}, \mathbf{c}')||\mathbf{h}_{\text{global}}). \quad (9)$$

Position-to-regional attention subsequently integrates the globally informed key features into regional tokens \mathbf{s} :

$$\text{Pos-to-Reg}(\mathbf{s}, \mathbf{h}'||\mathbf{c}', \mathbf{h}'||\mathbf{c}') = \text{Softmax} \left(\frac{\mathbf{W}'_Q \mathbf{s} (\mathbf{W}'_K \cdot \mathbf{h}'||\mathbf{c}')^\top}{\sqrt{d}} \right) \mathbf{W}'_V \cdot \mathbf{h}'||\mathbf{c}', \quad (10)$$

$$\mathbf{s}' = \mathbf{s} + \text{Pos-to-Reg}(\mathbf{s}, \mathbf{c}'||\mathbf{p}', \mathbf{c}'||\mathbf{p}'). \quad (11)$$

with distinct learnable projections \mathbf{W}'_Q , \mathbf{W}'_K , and \mathbf{W}'_V . This two-step attention mechanism ensures that synoptic-scale dynamics are effectively integrated into high-resolution regional features, enabling globally consistent and locally accurate weather prediction.

Global token adaptation with regional feedback. To enable large-scale dynamics to adapt to regional details, global tokens spatially aligned with regional tokens ($\mathbf{S}_{\text{aligned}}$) are updated via token-wise concatenation and an adapter MLP:

$$\mathbf{S}'_{\text{aligned}} = \text{Concat}(\mathbf{S}_{\text{aligned}}, \mathbf{s}') \in \mathbb{R}^{n \times 2d}, \quad (12)$$

$$\mathbf{S}''_{\text{aligned}} = \mathbf{S}_{\text{aligned}} + \text{MLP}_{\text{Adapter}}(\mathbf{S}'_{\text{aligned}}). \quad (13)$$

These adapted tokens $\mathbf{S}''_{\text{aligned}}$ replace their counterparts in the global token sequence, allowing regional fine-scale information to recursively influence the global context in subsequent encoder layers.

3.4 Model Optimization

The optimization schedule follows a three-stage training protocol: (1) global model pretraining, (2) regional model one-step training (6-hours ahead), and (3) regional model autoregressive roll-out fine-tuning (12 ~ 48-hours ahead).

Training objective. For global model pretraining, we employ the weighted mean absolute error (MAE) across multivariate atmospheric states. Decomposing the weather state \mathbf{U}^t into surface-level variables and upper-air atmospheric variables, $\hat{\mathbf{U}}^t = (\hat{\mathbf{S}}^t, \hat{\mathbf{A}}^t)$ and $\mathbf{U}^t = (\mathbf{S}^t, \mathbf{A}^t)$, the loss can be written as:

$$\mathcal{L}(\hat{\mathbf{U}}, \mathbf{U}^t) = \frac{1}{V_S + V_A} \left[\left(\sum_{k=1}^{V_S} \frac{w_k^S}{H \times W} \sum_{i=1}^H \sum_{j=1}^W |\hat{S}_{i,j,k}^t - S_{i,j,k}^t| \right) + \left(\sum_{k=1}^{V_A} \frac{1}{H \times W \times P} \sum_{p=1}^P w_{c,k}^A \sum_{i=1}^H \sum_{j=1}^W |\hat{A}_{i,j,p,k}^t - A_{i,j,p,k}^t| \right) \right], \quad (14)$$

where V_A and V_S are numbers of upper-air and surface variables, P is the number of pressure levels, w_k^S is the weight associated with surface-level variable k , and $w_{c,k}^A$ is the weight associated with atmospheric variable k at pressure level p .

During both one-step training and roll-out fine-tuning of regional model, we directly using MAE as the objective:

$$\mathcal{L}(\hat{\mathbf{u}}, \mathbf{u}^t) = \frac{1}{V_{\text{reg}}} \left(\sum_{k=1}^{V_{\text{reg}}} \frac{1}{h \times w} \sum_{i=1}^h \sum_{j=1}^w |\hat{u}_{i,j,k}^t - u_{i,j,k}^t| \right), \quad (15)$$

where V_{reg} is the number of variables in regional analyses.

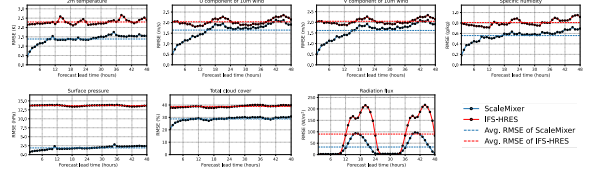
Roll-out Fine-tuning. The model makes forecasts for the next 6 hours in one step, and longer forecasts are obtained by rolling auto-regressively, which may suffer from error accumulations. To enhance the multi-step forecasting accuracy, we adopt a rolling-out fine-tuning strategy for 48 hours. It is performed by predicting $\hat{\mathbf{U}}^{t_0+6(n+1)+6H}$ and $\{\hat{\mathbf{u}}^{t_0+6(n+1)+iH}\}_{i=1}^6$ with the predictions from the previous step $\hat{\mathbf{U}}^{t_0+6n+6H}$ and $\{\hat{\mathbf{u}}^{t_0+6n+iH}\}_{i=1}^6$ as input, for $n = 0, 1, \dots$ recursively, and optimize the loss function of 3.4 and 3.4 over the 48 time spans.

Implementation and Training Details. The global Transformer encoder comprises 24 layers ($M = 24$), while the regional encoder and ScaleMixer modules each contain 4 layers ($k = 4$). The model employs a hidden dimension of 1536 and identifies $m = 64$ key positions for cross-scale interaction in each ScaleMixer module. The framework contains 1.07 billion parameters, with the global model $\mathcal{M}_{\text{global}}$ accounting for 736 million. Full implementation details are summarized in Section A.

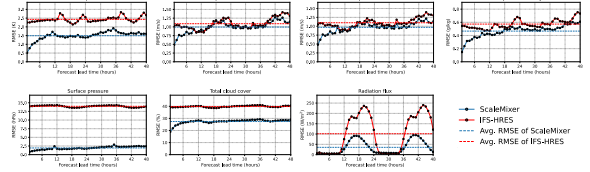
The global model was pretrained for 150,000 steps on $32 \times$ NVIDIA A800 GPUs using the AdamW optimizer [19] with a per-GPU batch size of 1. A cosine learning rate schedule was applied with linear warmup over 1,000 steps, decaying from 7×10^{-4} to 1×10^{-7} . Regional model training followed identical hyperparameters over 80,000 iterations on $8 \times$ A800 GPUs, with $\mathcal{M}_{\text{global}}$ parameters frozen. During regional roll-out fine-tuning, the model was trained for 100,000 steps at a fixed learning rate of 1×10^{-6} . The one-time training takes approximately 20 days on 8 NVIDIA A800 GPUs, and the inference stage is quite efficient, taking less than 3 minutes for 48-hour forecasting on a single GPU.

4 Experiments

To resolve high-impact meteorological phenomena such as convective storms and boundary layer dynamics, weather prediction



(a) Latitude-weighted RMSE for 7 surface variables (2024/10–2024/12 hindcast period)



(b) Latitude-weighted RMSE for 7 surface variables (2025/01–2025/04 operational period)

Figure 2: ScaleMixer demonstrates superior deterministic forecasting skill compared to IFS-HRES at 0.05° resolution. Seven surface variables (T2M, U10, V10, Q, P, TCC, and SSRD) are evaluated using latitude-weighted RMSE (lower values indicate superior performance). (a) Hindcast results show ScaleMixer outperforms IFS-HRES across all variables during 2024/10–2024/12. (b) Operational forecasts confirm ScaleMixer maintains superiority performance (2025/01–2025/04).

systems require high-resolution spatial-temporal modeling capabilities. We evaluate ScaleMixer through two complementary experimental paradigms: (1) *hindcast* for verification using reanalysis data, and (2) *operational forecast* to assess predictive skill under dynamically evolving initial conditions consistent with production environment management system.

4.1 Datasets

Global Reanalysis (ERA5). The European Centre for Medium-Range Weather Forecasts (ECMWF) ERA5 reanalysis provides 0.25° horizontal resolution (1440×720 latitude-longitude grid) atmospheric states with 37 hybrid pressure levels. Spanning 1979–2015, this dataset serves as the primary training source for the global model ($\mathcal{M}_{\text{global}}$), with 2016 reserved for validation. ERA5’s spatiotemporal continuity and multivariate fidelity make it a standard for data-driven weather modeling [12]. Similar to most AI-based weather forecasting foundation models, we select 5 atmospheric variables (u-component of wind speed, v-component of wind speed, temperature, specific humidity, geopotential) at 13 pressure levels (50 hPa, 100 hPa, 150 hPa, 200 hPa, 250 hPa, 300 hPa, 400 hPa, 500 hPa, 600 hPa, 700 hPa, 850 hPa, 925 hPa, 1000 hPa), 6 surface variables and 6 static variables from the raw ERA5 dataset, and use z-score normalization for each variable. All variables are inputs of $\mathcal{M}_{\text{global}}$, and all variables except the static ones are used as model outputs.

Global Operational Analysis. Operational analysis utilize the initial conditions from ECMWF’s High-Resolution Deterministic Prediction (HRES) system, which assimilates observations through

Table 1: Average RMSE and ACC across $\Delta t = 1 \sim 48$ hours lead time regional weather hindcast at 0.05° resolution. The best results are bolded.

Variable	Latitude-weighted RMSE								Latitude-weighted ACC						
	IFS-HRES	Baguan	M_{global}	M_{regional}	OneForecast	LAM	ScaleMixer	Δ RMSE	IFS-HRES	M_{global}	M_{regional}	OneForecast	LAM	ScaleMixer	Δ ACC
T2M	1.815	1.928	1.991	2.452	1.571	1.742	1.382	↓23.86%	0.862	0.881	0.845	0.897	0.901	0.921	↑6.84%
U10	1.934	1.956	1.967	2.631	2.251	1.889	1.644	↓14.99%	0.721	0.753	0.716	0.744	0.742	0.793	↑9.99%
V10	1.928	1.937	1.970	2.886	2.316	1.905	1.617	↓16.13%	0.723	0.751	0.713	0.732	0.737	0.785	↑8.57%
Q	0.807	0.611	0.811	1.243	0.714	0.676	0.559	↓30.73%	0.774	0.768	0.771	0.751	0.781	0.812	↑4.91%
P	13.27	22.97	10.27	4.241	2.545	2.14	1.874	↓85.88%	0.887	0.902	0.894	0.899	0.912	0.920	↑3.72%
TCC	38.83	31.83	(N/A)	43.71	37.74	34.13	28.76	↓25.93%	0.563	(N/A)	0.617	0.621	0.679	0.721	↑28.06%
SSRD	51.25	41.18	(N/A)	68.42	52.56	42.41	33.26	↓34.04%	0.824	(N/A)	0.834	0.838	0.850	0.887	↑7.64%

(1) Δ RMSE and Δ ACC denote RMSE and ACC improvement of ScaleMixer compared to IFS-HRES. (2) M_{global} denotes standalone global model, and M_{regional} denotes uncoupled regional model. (3) Results of IFS-HRES (0.1°) and Baguan, and M_{global} (0.25°) are corrected and downscaled to target grid (0.05°) using a pretrained bias-correction and downscaling model (based on a ViT backbone trained on ERA5 and CLDAS data) for comparison. (4) T2M: 2m temperature; U10/V10: 10m wind components; Q: Specific humidity; P: Surface Pressure; TCC: Total cloud cover; SSRD: Radiation flux (surface solar radiation downward).

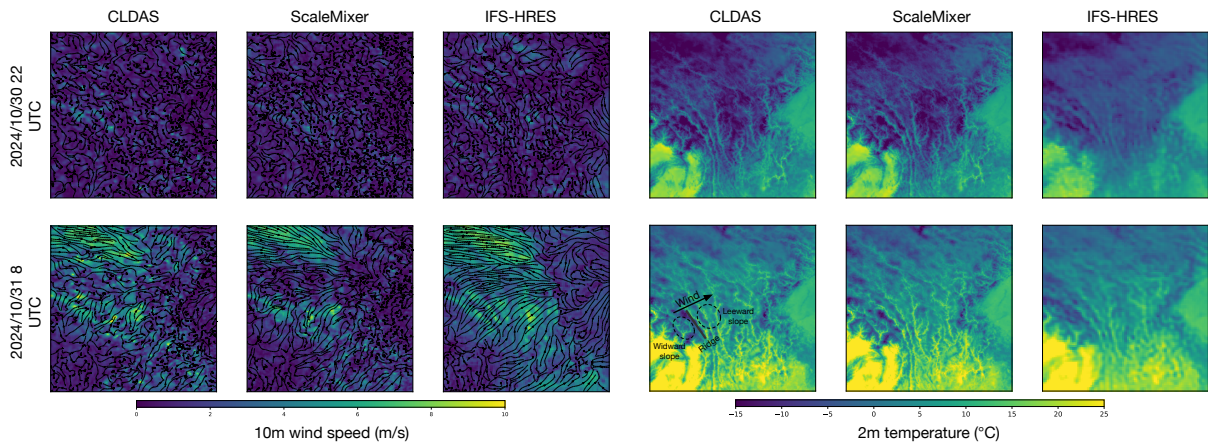


Figure 3: Left: Temporal evolution of 10m wind speed predictions initialized at 2024/10/30 12 UTC over the Hengduan Mountains ($25.0\text{--}35.0^\circ\text{N}$, $95.0\text{--}105.0^\circ\text{E}$), China. Black arrows represent wind flow fields. ScaleMixer resolves enhanced resolution of orographic wind heterogeneity (peaking >10 m/s at crests and <2 m/s in valleys). Right: Corresponding temperature fields. Foehn effects are illustrated in the picture, characterized by $4\text{--}8^\circ\text{C}$ leeward warming relative to windward slopes through adiabatic compression processes. ScaleMixer captures fine-grained temperature gradients, contrasting with IFS-HRES exhibiting spatial smoothing forecasts.

4D-variational data assimilation [27]. The 0.1° analysis fields (interpolated to ERA5 resolution, 0.25°) provide dynamically real-time initial conditions for ScaleMixer’s operational deployment during 2025/01–2025/04.

Regional Analysis (CLDAS). The China Meteorological Administration’s Land Data Assimilation System (CLDAS) is a near-realtime regional reanalysis product. It contains 7 critical surface variables with 1 hour intervals, covering East Asia ($0\text{--}65^\circ\text{N}$, $60\text{--}160^\circ\text{E}$) area at a spatial resolution of 0.01° . To reduce computational complexity and maintain detailed information, we interpolate the data to 0.05° latitude-longitude gridding. The full dataset covers from 2020 onward. We use data from 2022/01–2024/09 for training the global-regional model ($M_{\text{global-regional}}$), with two independent evaluation periods defined as: **Hindcast evaluation** (ERA5 input):

2024/10–2024/12 and **Operational evaluation** (operational analysis input): 2025/01–2025/04. All raw variables are also z-score normalized before fed into the model.

More details of datasets and experimental settings can be found in Section B.

4.2 Evaluation Metrics and Baselines

Evaluation metrics. To measure the performance of regional weather forecasting, we evaluate all methods using latitude-weighted root mean squared error (RMSE) and latitude-weighted anomaly correlation coefficient (ACC). More details of metrics can be found in Section C.

Baselines. We comprehensively evaluate ScaleMixer against several strong baselines: (1) our internal global model (M_{global}); (2) a standalone regional model initialized from CLDAS data without global coupling (M_{regional}); (3) an AI-based global forecast model

Baguan [22], which demonstrates superior performance among a set of state-of-the-art data-driven weather models on Weather-Bench¹ and provides more comprehensive surface meteorological variables than other global models like Pangu-Weather [2] and GraphCast [17] (detailed comparisons can be found in Section F); (4) the operational high-resolution NWP system IFS-HRES from ECMWF [9], which serves as a gold-standard reference. The resolutions of AI-based global forecasts and IFS-HRES are 0.25° and 0.1° , respectively, and there may exist systematic bias between their forecast values and CLDAS. For a fair comparison, we employ a downscaling and correction model to map the original forecast values to the target 0.05° grids. The downscaling and correction model is trained on ERA5 and CLDAS, using Swin Transformer [18] as the backbone, containing 4 layers block and a hidden dimension of 192; (5) OneForecast [11], which introduces a Neural Nested Grid method that typically passes boundary feature maps between grids of different resolutions via direct interpolation and concatenation; and (6) Limited Area Model (LAM), which is built upon $M_{regional}$ (Standalone Regional Model) but enhanced to take both regional initial conditions and external global forecasts as input.

4.3 Skillful Regional Weather Forecasting at 0.05° Resolution

We focus on short-term forecasting for next 48 hours, primarily because such outlooks have a more immediate impact on societal functions and daily routines. Furthermore, this is the period that NWP models have optimal performances. The deterministic forecasting results of ScaleMixer and baselines are summarized in Table 1, and Figure 2, evaluating forecast skill across $\Delta t = 1 \sim 48$ hours lead time.

Hindcast evaluation. For the ERA5-driven hindcast period (2024/10 – 2024/12), ScaleMixer achieves significant improvements across all seven surface variables (T2M, U10, V10, Q, P, TCC, and SSRD) compared to both standalone global/regional baselines and IFS-HRES (Table 1), verifying the effectiveness of coupling global and regional scales. ScaleMixer achieves 40.86% lower latitude-weighted RMSE and 9.96% higher ACC compared to IFS-HRES, indicating enhanced resolution capability for mesoscale convective systems and boundary layer dynamics. As shown in Figure 2a, performance advantages persist consistently across forecast horizons.

Operational forecast evaluation. Under dynamically evolving operational initial conditions (2025/01–2025/04), ScaleMixer maintains superior skill despite real-time analysis field uncertainties (Figure 2b). Compared to IFS-HRES at 0.1° resolution, statistically significant RMSE improvements are sustained through 48-hour lead times under operational constraints, with pronounced improvements in 1–24-hours ahead predictions where regional-scale processes dominate.

Evaluation against station observations. Although we have used downscaling models to map IFS-HRES to CLDAS, there may still exist some fairness concerns since ScaleMixer is end-to-end trained on the ground truth. We make extensive comparisons against station observations, which is more fair. The real-time station observation

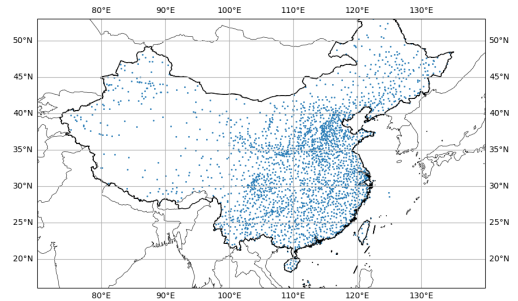


Figure 4: Station distribution map. The station observation dataset contains 2216 weather stations across China, which record hourly observations of meteorological variables such as temperature, air pressure, and wind speed.

dataset is a product provided by China Meteorological Administrations. It contains more than 2000 stations distributed across China, with a portion located in complex terrain areas such as plateaus and mountainous regions, as shown in Figure 4. These stations have undergone quality control and provide hourly observations of several meteorological variables. We focus on some key variables with high importance for downstream usages and provided in our model: 2m temperature (T2M), 2m dewpoint temperature (D2M) and 10m wind speed (WS10). In implementation, we interpolate the grid predictions of ScaleMixer and IFS-HRES to stations according to their latitudes and longitudes. Table 2 shows the RMSE of IFS-HRES, Baguan and ScaleMixer. Compared to IFS-HRES and Baguan, ScaleMixer achieves an average improvement of 27.63% across the three meteorological variables.

Table 2: Average RMSE across $\Delta t = 1 \sim 48$ hours lead time regional weather operational forecasting against weather station observations.

Variable	IFS-HRES	Baguan	ScaleMixer	Δ RMSE
T2M	3.158	3.108	1.822	↓41.4%
D2M	2.812	2.655	1.789	↓36.4%
WS10	1.401	1.402	1.329	↓5.10%

4.4 Case Studies

Orographic-induced wind and temperature. As exemplified in Figure 3 (left) for wind prediction of the complex terrain regions in the Hengduan Mountains ($25.0\text{--}35.0^\circ\text{N}$, $95.0\text{--}105.0^\circ\text{E}$) China, ScaleMixer (0.05°) resolves wind characteristics across topographic gradients: maximum wind speed at mountain crests (exceeding 10 m/s) and deceleration within valleys (<2 m/s). This contrasts with IFS-HRES (0.1°) which exhibits systematic underestimation of orographic wind characteristics due to insufficient subgrid-scale orographic parametrization.

¹<https://sites.research.google/gr/weatherbench/scorecards-2020/>

Table 3: Ablation study of ScaleMixer components on 48-hour forecast performance.

Model Variant	Configuration Details	T2M RMSE	U10 RMSE
ScaleMixer	Adaptive Sampling + Bidirectional	1.382	1.644
Variant A	Random Sampling + Bidirectional	1.605 (+16.1%)	1.882 (+14.5%)
Variant B	Fixed Uniform Grid + Bidirectional	1.512 (+9.4%)	1.795 (+9.2%)
Variant C	Adaptive Sampling + Unidirectional	1.468 (+6.2%)	1.721 (+4.7%)
Variant D	No Interaction (Standalone)	1.991 (+44.1%)	1.967 (+19.6%)

Moreover, the same orographic forcing that generates wind heterogeneity also drives temperature variations. ScaleMixer resolves pronounced temperature contrasts across elevation gradients (Fig. 3, right), with leeward slopes exhibiting 4–8°C warming relative to windward sides, a canonical Föhn effect signature², arising from adiabatic compression of descending air masses. In contrast, IFS-HRES underestimates these temperature gradients, failing to capture dependencies between terrain steepness and temperature variation. The enhanced resolution with data-driven method in ScaleMixer enables superior representation fine-grained weather features in complex terrain.

Additional visualizations of forecasts are provided in Section E, which demonstrate the framework’s capability to capture high-resolution meteorological details.

4.5 Ablation Studies

To rigorously validate the architectural design of ScaleMixer, we conducted fine-grained ablation studies focusing on two core dimensions: the sampling strategy for key position identification and the directionality of cross-scale coupling. Furthermore, we analyzed the sensitivity of the model to critical hyperparameters. All ablation experiments were conducted on the validation set with a forecast lead time of $\Delta t = 24$ hours.

Effectiveness of ScaleMixer Components. We compared our proposed framework against four variants: (A) *Random Sampling*, replacing adaptive identification with random selection; (B) *Fixed Uniform Grid*, utilizing a static grid for interaction; (C) *Unidirectional Coupling*, allowing only global-to-regional information flow; and (D) *No Interaction*, equivalent to the standalone regional model. The results are summarized in Table 3.

The results demonstrate: (1) **Effectiveness of Adaptive Sampling:** The proposed adaptive key position identification significantly outperforms the Fixed Uniform Grid (Variant B), reducing T2M RMSE by 9.4%. This demonstrates that dynamically focusing computation on meteorologically active regions (e.g., high-gradient boundaries) is far more efficient than uniform processing, which may waste capacity on static areas; and (2) **Effectiveness of Bidirectional Coupling:** Compared to unidirectional coupling (Variant C), our bidirectional mechanism achieves a 6.2% improvement in T2M RMSE. This confirms that allowing high-resolution regional features to explicitly refine global tokens creates a necessary closed-loop feedback, enhancing the consistency of the synoptic-scale context.

Hyperparameter Sensitivity. We further investigated the sensitivity of the regional encoder depth (k). As shown in Table 5, increasing the number of layers from $k = 2$ to $k = 4$ yields significant gains, while $k = 8$ offers diminishing returns with doubled computational cost. Based on these results, we adopted $k = 4$ as the default configuration to balance forecasting accuracy and inference efficiency.

Table 4: Sensitivity analysis of Regional Encoder Layers (k).

Metric	Regional Encoder Layers (k)		
	$k = 2$	$k = 4$	$k = 8$
T2M RMSE	1.485	1.382	1.379
U10 RMSE	1.752	1.644	1.641
<i>Inference Time</i>	<i>22ms</i>	<i>28ms</i>	<i>51ms</i>

5 Conclusion

In this paper, we present a multiscale deep learning framework for high-resolution regional weather forecasting that bridges synoptic-scale dynamics with localized mesoscale processes. By integrating a pretrained global foundation model and a novel bidirectional global-regional coupling module, ScaleMixer achieves state-of-the-art performance in resolving complex weather phenomena at 0.05° (~ 5 km) resolution. Experimental results establish ScaleMixer as a robust data-driven approach for regional weather forecasting. In the future, we will extend the framework to probabilistic forecasting and assimilate multi-modal observations (e.g., radar, satellite) for real-time forecasting.

Limitations and Ethical Considerations

Limitations. While ScaleMixer demonstrates significant advancements in regional weather forecasting, it is a purely data-driven model and lacks explicit equation-based constraints (e.g., Navier–Stokes or hydrostatic balance), which can cause unphysical artifacts in long roll-outs, especially in extreme regimes. Future work will add physics-informed regularization to better enforce conservation laws.

Ethical Considerations Both global reanalysis and global operational analysis data are publicly available. The CLDAS dataset and weather station observations were obtained from the China Meteorological Administration, and we have been granted permission to use them for academic research, which poses no potential ethical risks.

²https://en.wikipedia.org/wiki/Foehn_wind

References

- [1] Simon Adamov, Joel Oskarsson, Leif Denby, Tomas Landelius, Kasper Hintz, Simon Christiansen, Irene Schicker, Carlos Osuna, Fredrik Lindsten, Oliver Fuhrer, et al. 2025. Building Machine Learning Limited Area Models: Kilometer-Scale Weather Forecasting in Realistic Settings. *arXiv preprint arXiv:2504.09340* (2025).
- [2] Kaifeng Bi, Lingxi Xie, Hengheng Zhang, Xin Chen, Xiaotao Gu, and Qi Tian. 2023. Accurate medium-range global weather forecasting with 3D neural networks. *Nature* 619, 7970 (2023), 533–538.
- [3] Zied Ben Bouallège, Mariana C. A. Clare, Linus Magnusson, Estibaliz Gascón, Michael Maier-Gerber, Martin Janoušek, Mark Rodwell, Florian Pinault, Jesper S. Dramsch, Simon T. K. Lang, Baudouin Raoult, Florence Rabier, Matthieu Chevalier, Irina Sandu, Peter Dueben, Matthew Chantry, and Florian Pappenberger. 2024. The Rise of Data-Driven Weather Forecasting: A First Statistical Assessment of Machine Learning–Based Weather Forecasts in an Operational-Like Context. *Bulletin of the American Meteorological Society* 105, 6 (2024), E864 – E883. doi:10.1175/BAMS-D-23-0162.1
- [4] Kang Chen, Tao Han, Junchao Gong, Lei Bai, Fenghua Ling, Jing-Jia Luo, Xi Chen, Leiming Ma, Tianning Zhang, Rui Su, et al. 2023. FengWu: Pushing the Skillful Global Medium-range Weather Forecast beyond 10 Days Lead. *arXiv preprint arXiv:2304.02948* (2023).
- [5] Lei Chen, Xiaohui Zhong, Feng Zhang, Yuan Cheng, Yinghui Xu, Yuan Qi, and Hao Li. 2023. FuXi: A cascade machine learning forecasting system for 15-day global weather forecast. *npj Climate and Atmospheric Science* 6, 1 (2023), 190.
- [6] Jean Coiffier. 2011. *Fundamentals of numerical weather prediction*. Cambridge University Press, Cambridge, New York.
- [7] Alexey Dosovitskiy, Lucas Beyer, Alexander Kolesnikov, Dirk Weissenborn, Xi-aohua Zhai, Thomas Unterthiner, Mostafa Dehghani, Matthias Minderer, Georg Heigold, Sylvain Gelly, et al. 2020. An image is worth 16x16 words: Transformers for image recognition at scale. *arXiv preprint arXiv:2010.11929* (2020).
- [8] Alexey Dosovitskiy, Lucas Beyer, Alexander Kolesnikov, Dirk Weissenborn, Xi-aohua Zhai, Thomas Unterthiner, Mostafa Dehghani, Matthias Minderer, Georg Heigold, Sylvain Gelly, Jakob Uszkoreit, and Neil Houlsby. 2021. An Image is Worth 16x16 Words: Transformers for Image Recognition at Scale. In *International Conference on Learning Representations*.
- [9] ECMWF. 2023. *IFS Documentation CY48R1*. ECMWF.
- [10] European Centre for Medium-Range Weather Forecasts. 2023. *Description of the Integrated Forecasting System (IFS)* (cycle 48r1 ed.). <https://www.ecmwf.int/en/publications/manuals/deterministic-model>
- [11] Yuan Gao, Hao Wu, Ruiqi Shu, Huanshuo Dong, Fan Xu, Rui Chen, Yibo Yan, Qingsong Wen, Xuming Hu, Kun Wang, et al. 2025. OneForecast: A Universal Framework for Global and Regional Weather Forecasting. *arXiv preprint arXiv:2502.00338* (2025).
- [12] Hans Hersbach, Bill Bell, Paul Berrisford, Shoji Hirahara, András Horányi, Joaquín Muñoz-Sabater, Julien Nicolas, Carole Peubey, Raluca Radu, Dinand Schepers, et al. 2020. The ERA5 global reanalysis. *Quarterly Journal of the Royal Meteorological Society* 146, 730 (2020), 1999–2049.
- [13] James Hurrell, Marika Holland, Peter Gent, Steven Ghan, Jennifer Kay, Paul Kushner, J-F Lamarque, William Large, D Lawrence, Keith Lindsay, et al. 2013. The community earth system model: a framework for collaborative research. *Bulletin of the American Meteorological Society* 94, 9 (2013), 1339–1360.
- [14] Ryan Keisler. 2022. Forecasting global weather with graph neural networks. *arXiv preprint arXiv:2202.07575* (2022).
- [15] Dmitrii Kochkov, Janni Yuval, Ian Langmore, Peter Norgaard, Jamie Smith, Griffin Mooers, Milan Klöwer, James Lottes, Stephan Rasp, Peter Düben, et al. 2024. Neural general circulation models for weather and climate. *Nature* 632, 8027 (2024), 1060–1066.
- [16] Remi Lam, Alvaro Sanchez-Gonzalez, Matthew Willson, Peter Wirnsberger, Meire Fortunato, Ferran Alet, Suman Ravuri, Timo Ewalds, Zach Eaton-Rosen, Weihua Hu, et al. 2023. Learning skillful medium-range global weather forecasting. *Science* 382, 6677 (2023), 1416–1421.
- [17] Remi Lam, Alvaro Sanchez-Gonzalez, Matthew Willson, Peter Wirnsberger, Meire Fortunato, Ferran Alet, Suman Ravuri, Timo Ewalds, Zach Eaton-Rosen, Weihua Hu, et al. 2023. Learning skillful medium-range global weather forecasting. *Science* 382, 6677 (2023), 1416–1421.
- [18] Ze Liu, Yutong Lin, Yue Cao, Han Hu, Yixuan Wei, Zheng Zhang, Stephen Lin, and Baining Guo. 2021. Swin transformer: Hierarchical vision transformer using shifted windows. In *Proceedings of the IEEE/CVF international conference on computer vision*. 10012–10022.
- [19] Ilya Loshchilov and Frank Hutter. 2017. Decoupled weight decay regularization. *arXiv preprint arXiv:1711.05101* (2017).
- [20] Morteza Mardani, Noah Brenowitz, Yair Cohen, Jaideep Pathak, Chieh-Yu Chen, Cheng-Chin Liu, Arash Vahdat, Mohammad Amin Nabian, Tao Ge, Akshay Subramaniam, et al. 2025. Residual corrective diffusion modeling for km-scale atmospheric downscaling. *Communications Earth & Environment* 6, 1 (2025), 124.
- [21] Thomas Nils Nipen, Håvard Homleid Haugen, Magnus Sikora Ingstad, Even Marius Nordhagen, Aram Farhad Shafiq Salihi, Paulina Tedesco, Ivar Ambjørn Seierstad, Jørn Kristiansen, Simon Lang, Mihai Alexe, et al. 2024. Regional data-driven weather modeling with a global stretched-grid. *arXiv preprint arXiv:2409.02891* (2024).
- [22] Peisong Niu, Ziqing Ma, Tian Zhou, Weiqi Chen, Lefei Shen, Rong Jin, and Liang Sun. 2025. Utilizing strategic pre-training to reduce overfitting: Baguan-a pre-trained weather forecasting model. In *Proceedings of the 31st ACM SIGKDD Conference on Knowledge Discovery and Data Mining V. 2*. 2186–2197.
- [23] Joel Oskarsson, Tomas Landelius, and Fredrik Lindsten. 2023. Graph-based neural weather prediction for limited area modeling. *arXiv preprint arXiv:2309.17370* (2023).
- [24] William Peebles and Saining Xie. 2023. Scalable diffusion models with transformers. In *Proceedings of the IEEE/CVF international conference on computer vision*. 4195–4205.
- [25] Ilan Price, Alvaro Sanchez-Gonzalez, Ferran Alet, Timo Ewalds, Andrew El-Kadi, Jacklynn Stott, Shakir Mohamed, Peter Battaglia, Remi Lam, and Matthew Willson. 2023. GenCast: Diffusion-based ensemble forecasting for medium-range weather. *arXiv preprint arXiv:2312.15796* (2023).
- [26] Haoyu Qin, Yungang Chen, Qianchuan Jiang, Pengchao Sun, Xiancai Ye, and Chao Lin. 2024. Metmamba: Regional weather forecasting with spatial-temporal mamba model. *arXiv preprint arXiv:2408.06400* (2024).
- [27] Florence Rabier and Zhiqun Liu. 2003. Variational data assimilation: theory and overview. In *Proc. ECMWF Seminar on Recent Developments in Data Assimilation for Atmosphere and Ocean, Reading, UK*. 29–43.
- [28] Stephan Rasp, Peter D Dueben, Sebastian Scher, Jonathan A Weyn, Soukayna Moutatid, and Nils Thuerey. 2020. WeatherBench: a benchmark data set for data-driven weather forecasting. *Journal of Advances in Modeling Earth Systems* 12, 11 (2020), e2020MS002203.
- [29] Ashish Vaswani, Noam Shazeer, Niki Parmar, Jakob Uszkoreit, Llion Jones, Aidan N Gomez, Łukasz Kaiser, and Illia Polosukhin. 2017. Attention is all you need. *Advances in neural information processing systems* 30 (2017).
- [30] Ruolan Xiang, Christian R Steger, Shuping Li, Loïc Pellissier, Silje Lund Sørlund, Sean D Willett, and Christoph Schär. 2024. Assessing the regional climate response to different Hengduan Mountains geometries with a high-resolution regional climate model. *Journal of Geophysical Research: Atmospheres* 129, 6 (2024), e2023JD040208.
- [31] Pengbo Xu, Xiaogu Zheng, Tianyan Gao, Yu Wang, Junping Yin, Juan Zhang, Xuanze Zhang, San Luo, Zhonglei Wang, Zhimin Zhang, et al. [n. d.]. YingLong-weather: AI-Based Limited Area Models for Forecasting. ([n. d.]).

A Implementation Details

In our multiscale regional weather forecasting framework, the backbones of the global model ($\mathcal{M}_{\text{global}}$) and regional model ($\mathcal{M}_{\text{regional}}$) are based on ViT [8]. The framework contains 1.07 billion parameters, with the global model $\mathcal{M}_{\text{global}}$ accounting for 736 million. The hyperparameter configurations of the model are summarized in Table 5.

B Dataset Details and Experimental Settings

In our experiments, we use the preprocessed ERA5 data from WeatherBench [28]. ERA5 is a well-acknowledged weather forecasting benchmark dataset and it is widely used in data-driven weather forecasting methods. WeatherBench processed the raw ERA5 dataset³, which includes 8 atmospheric variables across 13 pressure levels, 6 surface variables, and 3 static variables. We normalize all the inputs via z-score normalization for each variable at each pressure level. Also, we apply the inverse normalization for the predictions of future states for performance evaluation.

We collected and processed operational analysis data, which are used for operational forecast, from initial conditions of ECMWF’s High-Resolution Deterministic Prediction (HRES) system, assimilating observations with 4D-variational data assimilation. The 0.1° analysis fields (interpolated to ERA5 resolution, 0.25°) provide dynamically real-time initial conditions. We set and process the atmosphere variables consistent with the ERA5 Dataset.

We also collected and processed the China Meteorological Administration’s Land Data System data (CLDAS), which offers 0.01° resolution meteorological fields over East Asia (0–65°N, 60–160°E). The regional analysis dataset is used to train and evaluate regional weather forecasting model. The dataset includes 7 critical surface variables: wind components (U, V), temperature (T), specific humidity (Q), pressure (P), radiation fluxes (SSRD), and total cloud cover (TCC). We normalize all the inputs via z-score normalization for each variable at each pressure level. Also, we apply the inverse normalization for the predictions of future states for performance evaluation.

B.1 ERA5 and operational analysis with 0.25° resolution

we selected 6 atmospheric variables at all **13 pressure levels**, 3 surface variables, and 3 static variables for the ERA5 dataset with 0.25° resolution, as detailed in Table 6. In our model training, we choose all variables as input variables, and all variables except three static variables as output variables that are used for loss calculation to pretrain global model $\mathcal{M}_{\text{global}}$.

B.2 CLDAS with 0.05° resolution

We selected 7 surface variables for the CLDAS dataset with 0.25° resolution, as detailed in Table 7. In our model training, we choose all variables as input variables, and all variables as output variables that are used for loss calculation to train global-regional model $\mathcal{M}_{\text{global-regional}}$.

³More details of ERA5 data can be found in <https://confluence.ecmwf.int/display/CKB/ERA5%3A+data+documentation>.

C Evaluation Metrics for Regional Weather Forecasting

This section provides detailed explanations of all the evaluation metrics for regional weather forecasting used in the main experiments. For each metric, \mathbf{u} and $\hat{\mathbf{u}}$ represent the predicted and ground truth values, respectively, both shaped as $h \times w \times V_{\text{reg}}$, where V_{reg} is the number of total weather factors, and $h \times w$ is the spatial resolution of latitude (h) and longitude (w). To account for the non-uniform grid cell areas, the latitude weighting term $\alpha(\cdot)$ is introduced.

Latitude-weighted Root Mean Square Error (RMSE). assesses model accuracy while considering the Earth’s curvature. The latitude weighting adjusts for the varying grid cell areas at different latitudes, ensuring that errors are appropriately measured. Lower RMSE values indicate better model performance.

$$\text{RMSE} = \frac{1}{V_{\text{reg}}} \sum_{k=1}^{V_{\text{reg}}} \sqrt{\frac{1}{hw} \sum_{i=1}^h \sum_{j=1}^w \alpha(i) (\hat{\mathbf{u}}_{i,j,k} - \mathbf{u}_{i,j,k})^2},$$

$$\alpha(i) = \frac{\cos(\text{lat}(i))}{\frac{1}{h} \sum_{i'=1}^h \cos(\text{lat}(i'))}.$$

Anomaly Correlation Coefficient (ACC). measures a model’s ability to predict deviations from the mean. Higher ACC values indicate better accuracy in capturing anomalies, which is crucial in meteorology and climate science.

$$\text{ACC} = \frac{\sum_{i,j,k} \hat{\mathbf{u}}'_{i,j,k} \mathbf{u}'_{i,j,k}}{\sqrt{\sum_{i,j,k} \alpha(h) (\hat{\mathbf{u}}'_{i,j,k})^2 \sum_{i,j,k} \alpha(h) (\mathbf{u}'_{i,j,k})^2}},$$

where $\mathbf{u}' = \mathbf{u} - C$ and $\hat{\mathbf{u}}' = \hat{\mathbf{u}} - C$, with climatology C representing the temporal mean of the same period over the training set.

D Broader Impacts

This research focuses on high-resolution regional weather forecasting, which has an essential influence on relevant fields such as energy, transportation, and agriculture. As an AI application for social good, our model boosts predictions for various weather factors such as temperature, wind speed, and radiation flux. It is essential to note that our work focuses solely on scientific issues, and we also ensure that ethical considerations are carefully taken into account. Thus, we believe that there is no ethical risk associated with our research.

E Visualization of Forecasts

To intuitively demonstrate the forecasting capacity of our model, we present the showcases of weather forecasting results in China and zoomed-in regions in Figures 5, 6, 7, 8, 9, 10, 11, 12, 13, 14, 15, and 16.

F Comparison with Weatherbench2’s Baselines

The global branch of our framework $\mathcal{M}_{\text{global}}$ demonstrates promising performance that aligns with top-tier AI weather models. Figure 17 shows RMSE and ACC for some key variables of our global

Table 5: Default hyperparameters of the framework.

Module	Hyperparameter	Description	Value
Global Model $\mathcal{M}_{\text{global}}$	P	Patch size of global tokens	6
	d	hidden dimension	1536
	M	Number of Transformer encoder layers of in the global model	24
	Heads	Number of attention heads	8
	MLP ratio	Expansion factor for MLP	4.
	Depth of prediction head	Number of deconvolution layers of the final prediction head	2
	Drop path	Stochastic depth rate	0.1
	Dropout	Dropout rate	0.1
Regional Model $\mathcal{M}_{\text{regional}}$	p	Patch size of regional tokens	30
	d	hidden dimension	1536
	k	Number of Transformer encoder layers of in the regional model	4
	Heads	Number of attention heads	8
	MLP ratio	Expansion factor for MLP	4.
	Depth of prediction head	Number of deconvolution layers of the final prediction head	2
	Drop path	Stochastic depth rate	0.1
	Dropout	Dropout rate	0.1
ScaleMixer	Depth	total number of ScaleMix modules	4
	Depth of position identification block	number of convolution layers in position identification block	1
	Kernel size	kernel size of convolution layers in position identification block	3
	m	number of key positions	64

model and Pangu-Weather [2], Fuxi [5], Graphcast [17] and IFS-HRES [9], reported on Weatherbench2⁴. It is evaluated on 2022 ERA5 dataset, with lead time ranging from 6 to 240 hours. For both surface variables and pressure level variables, our model outperforms Pangu-Weather, Graphcast and EC-IFS and is comparable to Fuxi in most cases. Notably, our global model achieves

an average improvement of 12.59%, 0.90%, 3.56%, 16.30% on RMSE over pangu-weather, fuxi, graphcast, EC-IFS, respectively, and an average improvement of 8.07%, 0.87%, 4.32%, 9.51% on ACC over pangu-weather, fuxi, graphcast, EC-IFS, respectively.

⁴<https://sites.research.google/gr/weatherbench/deterministic-scores/>

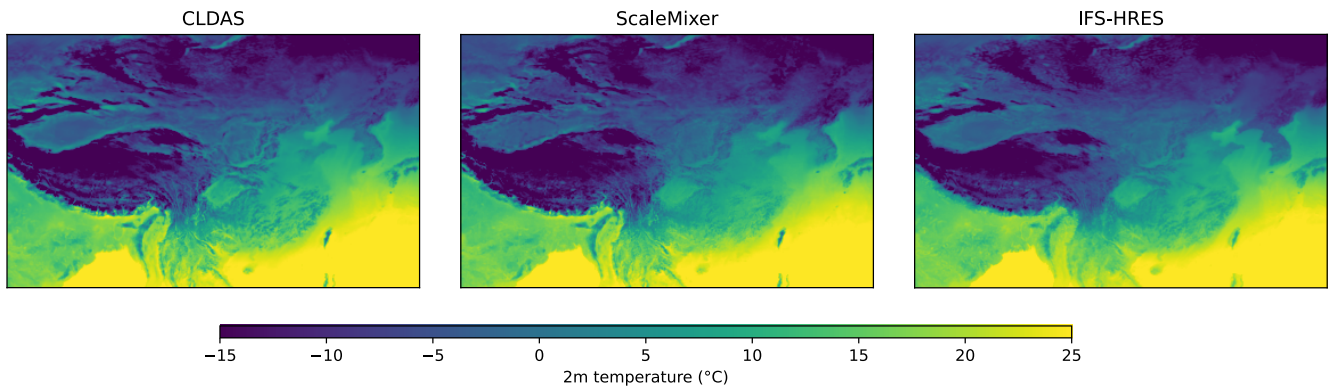
Table 6: Summary of ECMWF variables utilized in the ERA5 and operational analysis dataset with 0.25° resolution. The variables *lsm* and *oro* are constant and invariant with time.

Type	Variable Name	Abbrev.	Description	Pressure Levels
Static Variable	Land-sea mask	<i>lsm</i>	Binary mask distinguishing land (1) from sea (0)	N/A
	Orography	<i>oro</i>	Height of Earth's surface	N/A
	Latitude	<i>lat</i>	Latitude of each grid point	N/A
Surface Variable	2 metre temperature	<i>t2m</i>	Temperature measured 2 meters above the surface	Single level
	10 metre U wind component	<i>u10</i>	East-west wind speed at 10 meters above the surface	Single level
	10 metre V wind component	<i>v10</i>	North-south wind speed at 10 meters above the surface	Single level
	Mean sea level pressure	<i>msl</i>	Pressure of the atmosphere adjusted to the height of mean sea level	Single level
	Surface pressure	<i>sp</i>	Pressure of the atmosphere on the surface of land, sea and in-land water	Single level
	2 metre dewpoint temperature	<i>d2m</i>	Temperature to which the air, at 2 metres above the surface of the Earth	Single level
Upper-air Variable	Geopotential	<i>z</i>	Height relative to a pressure level	50, 100,150, 200, 250,300, 400, 500, 600, 700, 850, 925,1000 hPa
	U wind component	<i>u</i>	Wind speed in the east-west direction	50, 100,150, 200, 250,300, 400, 500, 600, 700, 850, 925,1000 hPa
	V wind component	<i>v</i>	Wind speed in the north-south direction	50, 100,150, 200, 250,300, 400, 500, 600, 700, 850, 925,1000 hPa
	Temperature	<i>t</i>	Atmospheric temperature	50, 100,150, 200, 250,300, 400, 500, 600, 700, 850, 925,1000 hPa
	Specific humidity	<i>q</i>	Mixing ratio of water vapor to total air mass	50, 100,150, 200, 250,300, 400, 500, 600, 700, 850, 925,1000 hPa

Table 7: Summary of variables utilized in CLDAS with 0.05° resolution.

Type	Variable Name	Abbrev.	Description
Surface Variable	2 metre temperature	<i>T</i>	Temperature measured 2 meters above the surface
	10 metre U wind component	<i>U</i>	East-west wind speed at 10 meters above the surface
	10 metre V wind component	<i>V</i>	North-south wind speed at 10 meters above the surface
	Surface specific humidity	<i>Q</i>	Mixing ratio of water vapor to total air mass at 2 meters above the surface
	Surface pressure	<i>P</i>	Pressure of the atmosphere on the surface of land, sea and in-land water
	Total cloud cover	<i>TCC</i>	Cloud occurring at different model levels through the atmosphere
	Radiation flux (surface solar radiation flux downwards)	<i>SSRD</i>	Flux of solar radiation that reaches a horizontal plane at the surface of the Earth

2024/11/19 23 UTC (Forecast lead time = 11)



2024/11/19 11 UTC (Forecast lead time = 23)

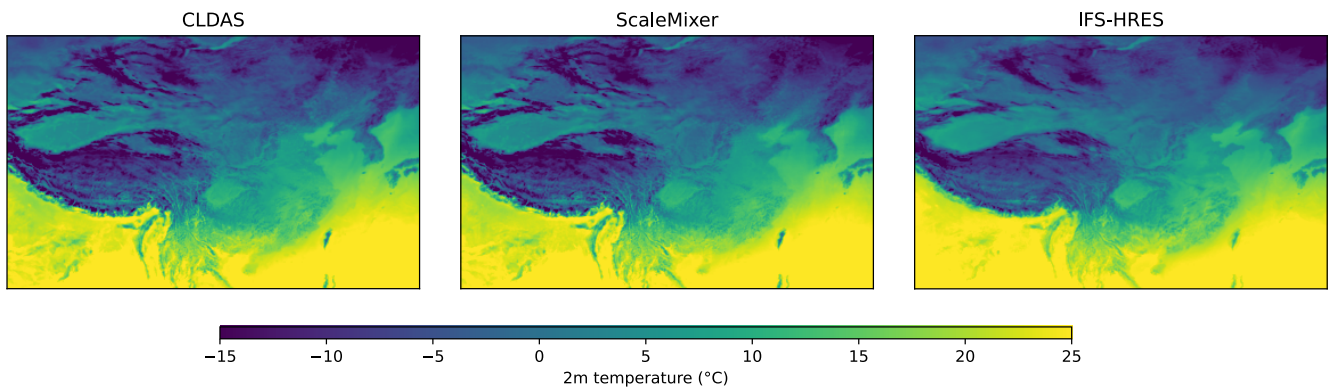
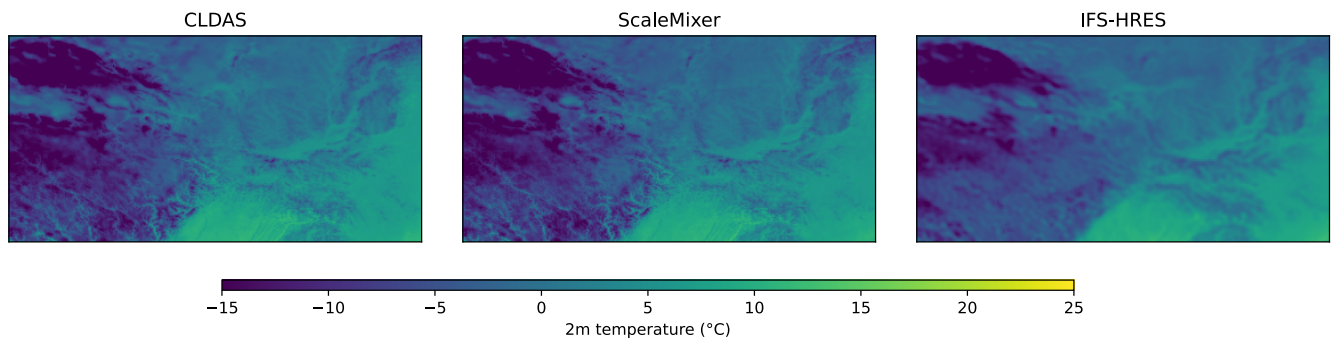


Figure 5: 2 metre temperature forecasts over China

2024/11/19 23 UTC (Forecast lead time = 11)



2024/11/19 11 UTC (Forecast lead time = 23)

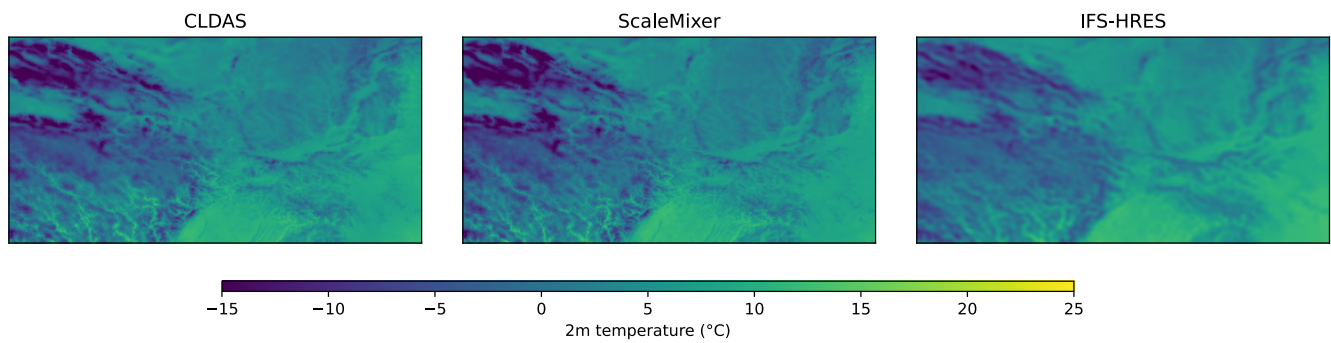
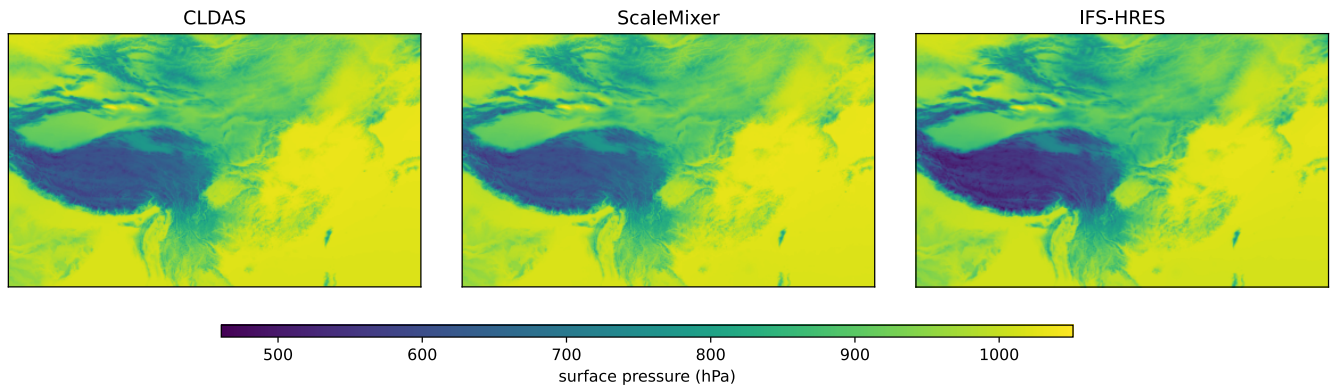


Figure 6: 2 metre temperature forecasts over a subregion of latitudes in [30, 40] and longitudes in [95, 115]

2024/11/19 23 UTC (Forecast lead time = 11)



2024/11/19 11 UTC (Forecast lead time = 23)

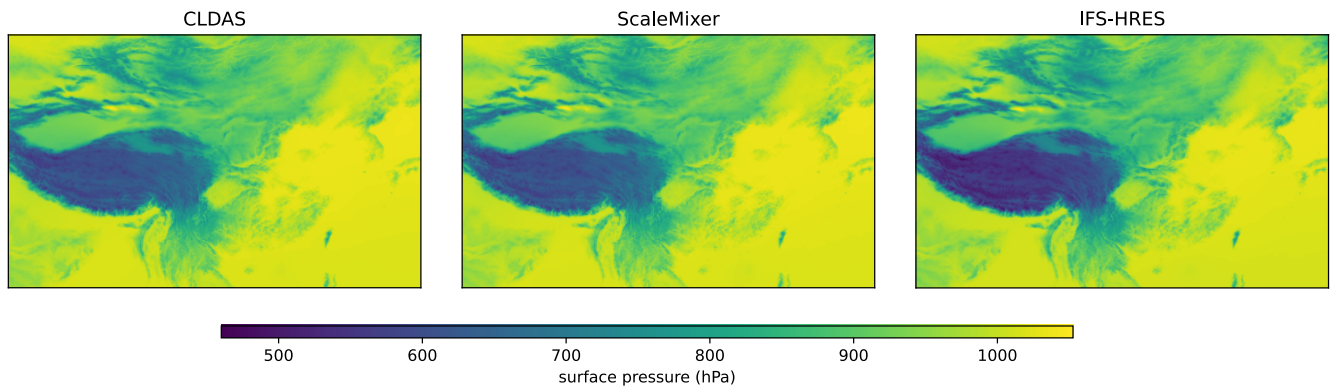
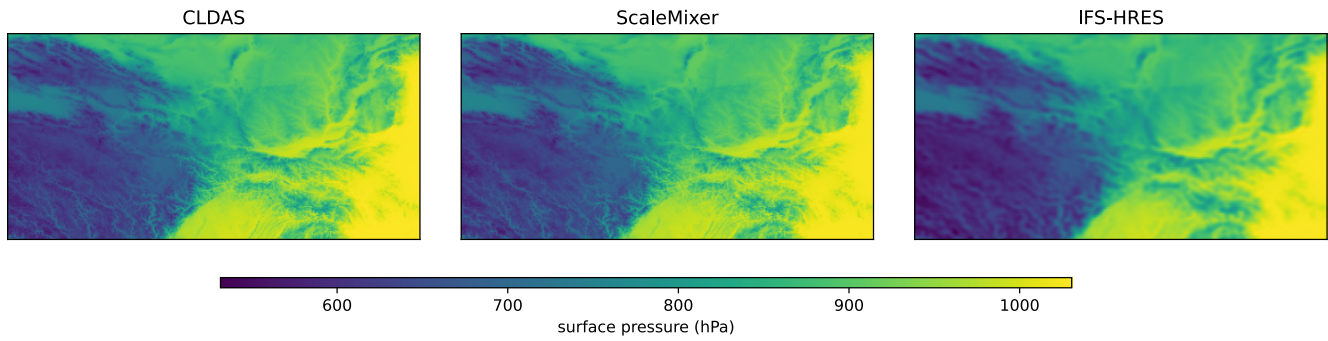


Figure 7: surface pressure forecasts over China

2024/11/19 23 UTC (Forecast lead time = 11)



2024/11/19 11 UTC (Forecast lead time = 23)

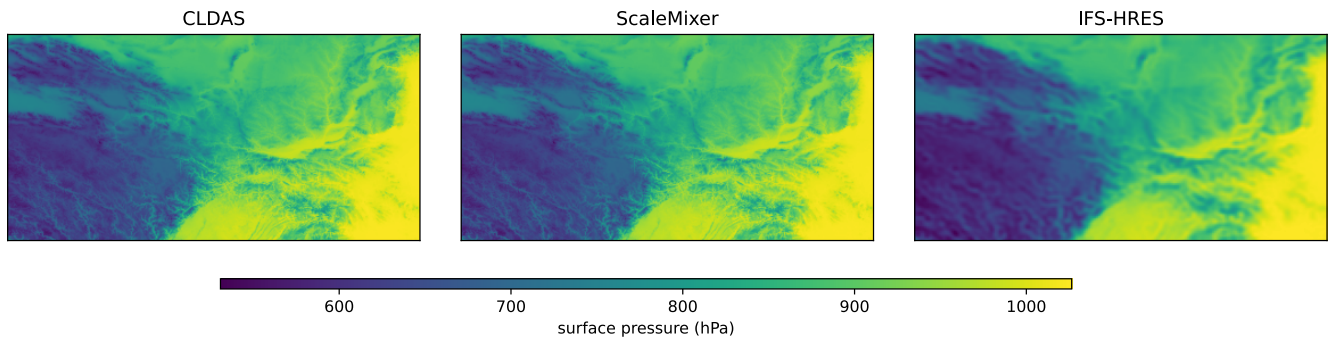
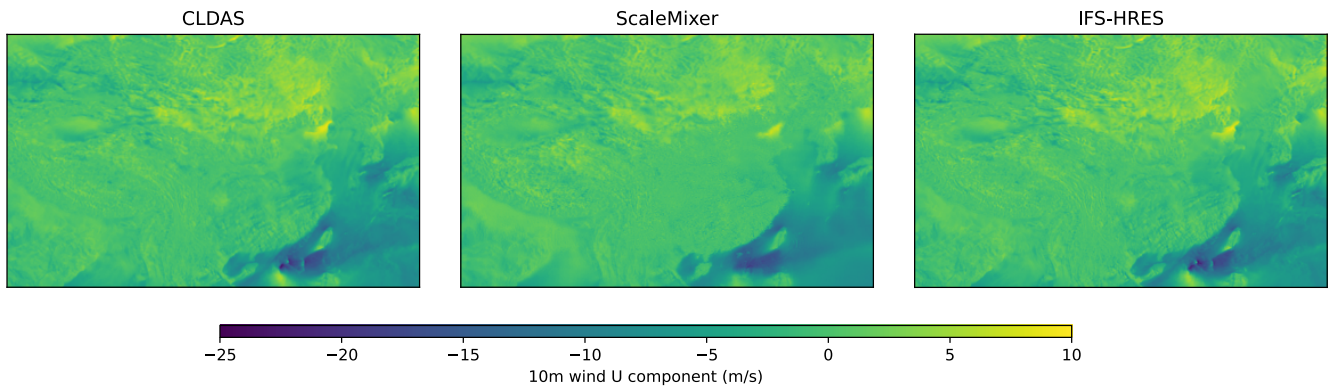


Figure 8: surface pressure forecasts over a subregion of latitudes in [30, 40] and longitudes in [95, 115]

2024/11/19 23 UTC (Forecast lead time = 11)



2024/11/19 11 UTC (Forecast lead time = 23)

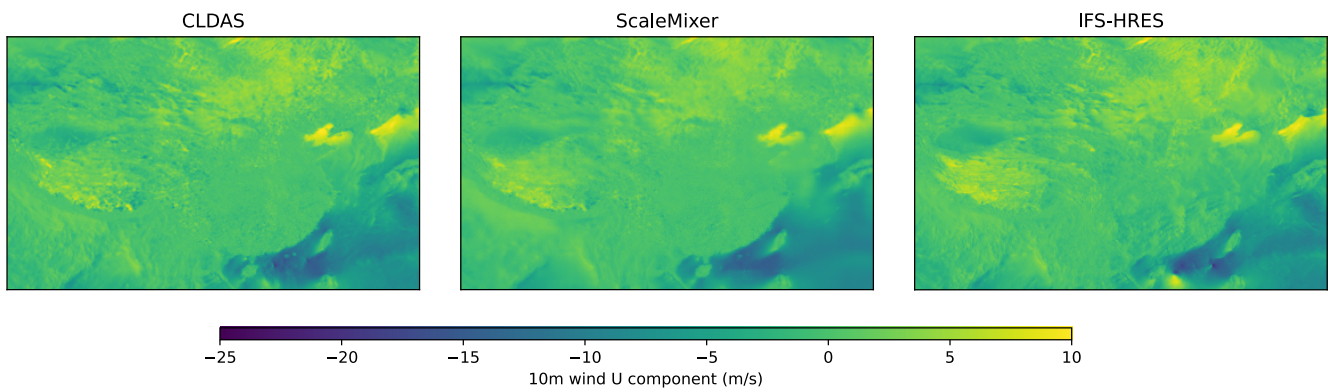


Figure 9: 10 metre Wind speed U component forecasts over China

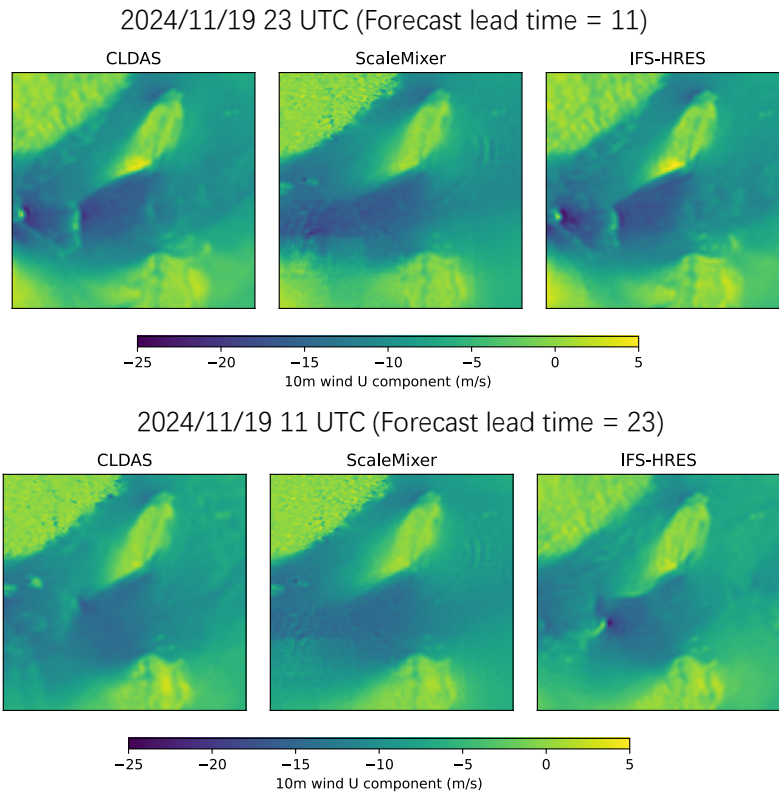
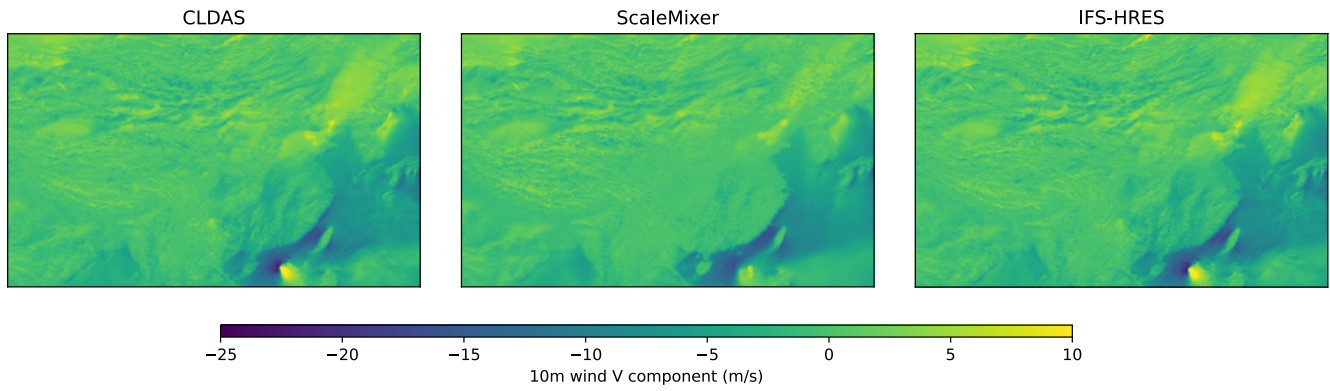


Figure 10: 10 metre wind speed U component forecasts over a subregion of latitudes in [16.3, 26] and longitudes in [115, 125]

2024/11/19 23 UTC (Forecast lead time = 11)



2024/11/19 11 UTC (Forecast lead time = 23)

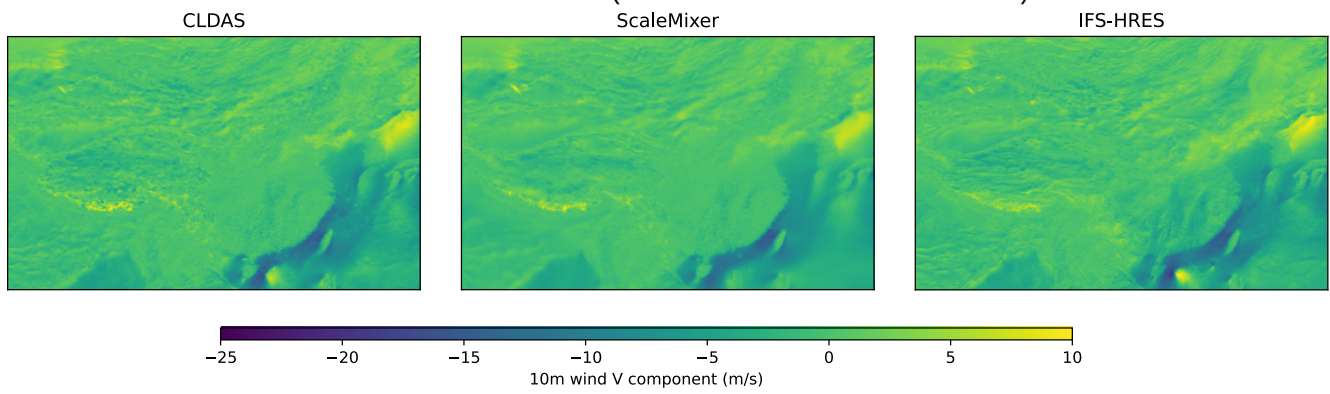


Figure 11: 10 metre Wind speed V component forecasts over China

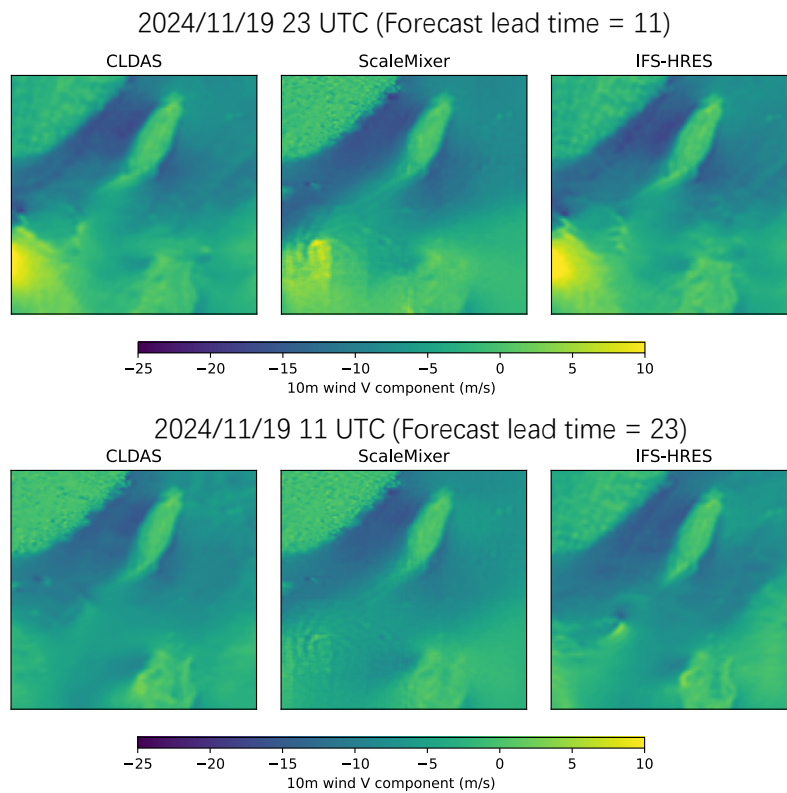
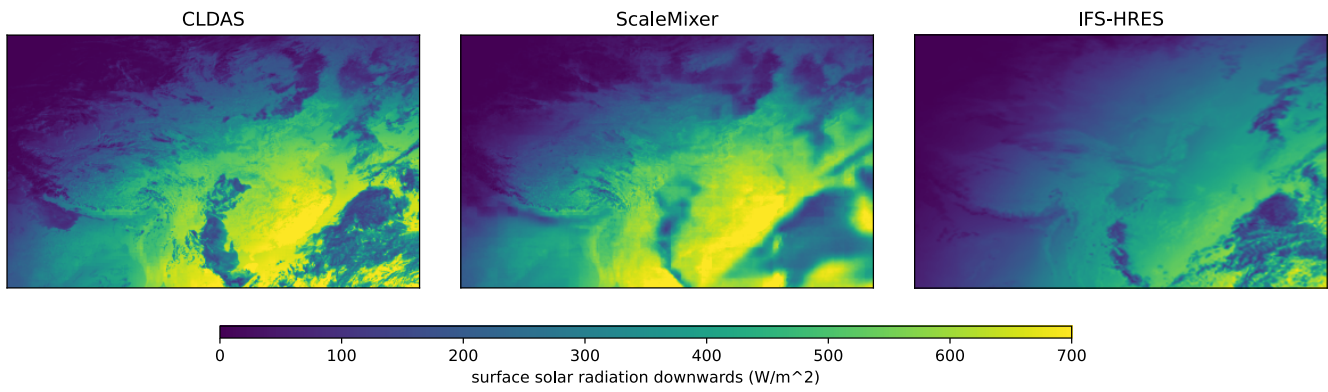


Figure 12: 10 metre wind speed V component forecasts over a subregion of latitudes in [16.3, 26] and longitudes in [115, 125]

2025/01/19 2 UTC (Forecast lead time = 14)



2025/01/19 4 UTC (Forecast lead time = 16)

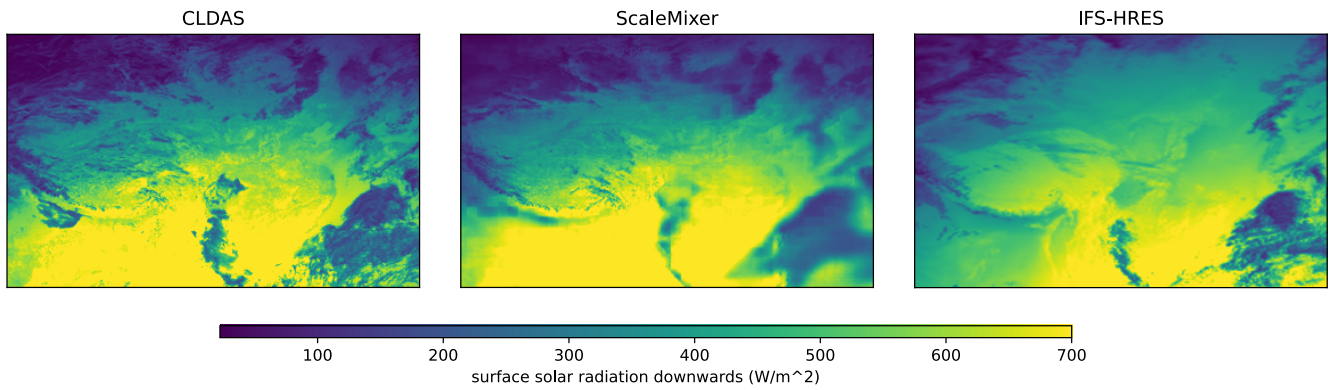
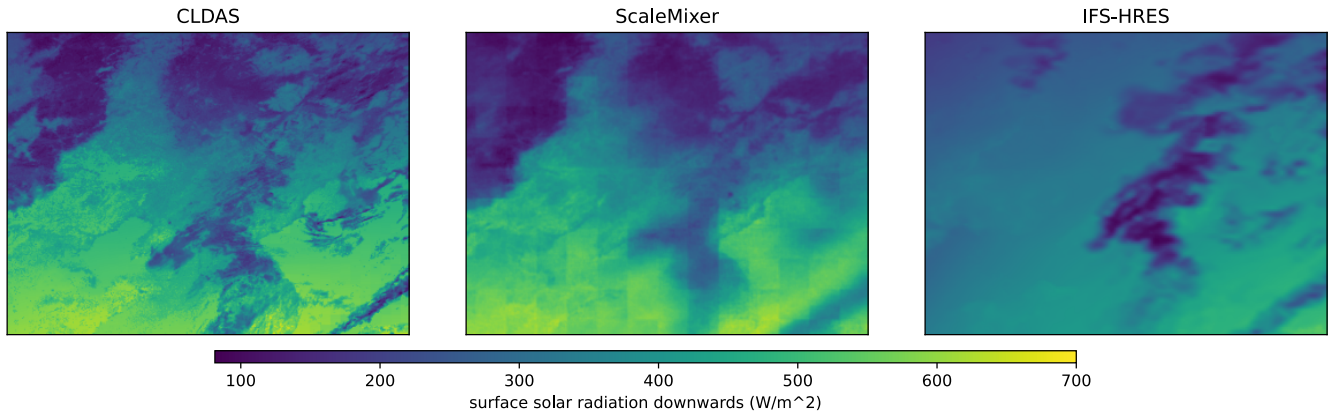


Figure 13: surface solar radiation downwards forecasts over China

2025/01/19 2 UTC (Forecast lead time = 14)



2025/01/19 4 UTC (Forecast lead time = 16)

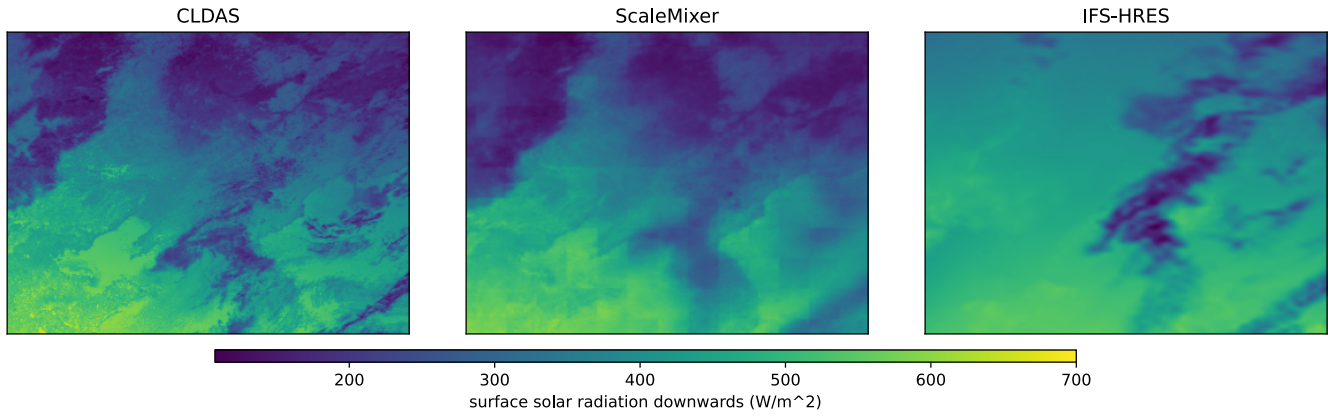
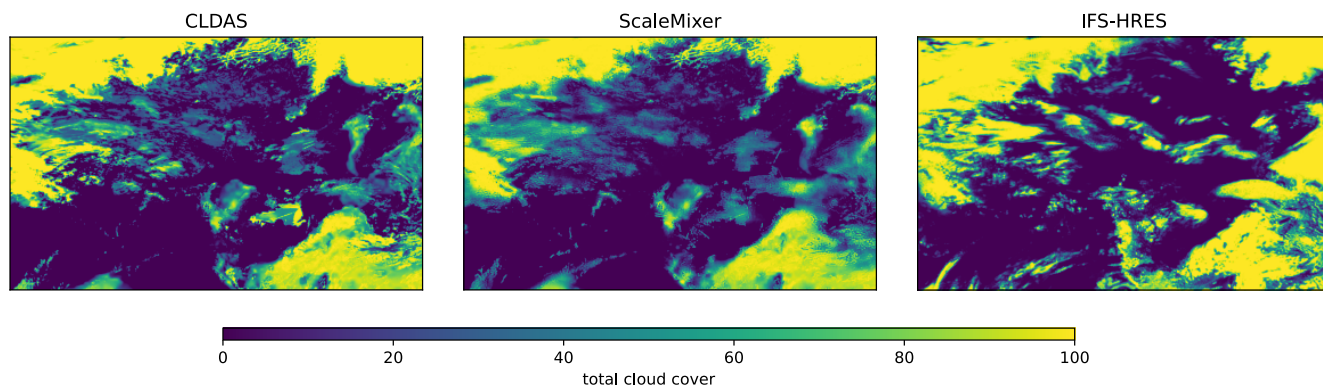


Figure 14: surface solar radiation downwards forecasts over a subregion of latitudes in [35, 50] and longitudes in [115, 135]

2025/01/18 13 UTC (Forecast lead time = 1)



2025/01/18 20 UTC (Forecast lead time = 8)

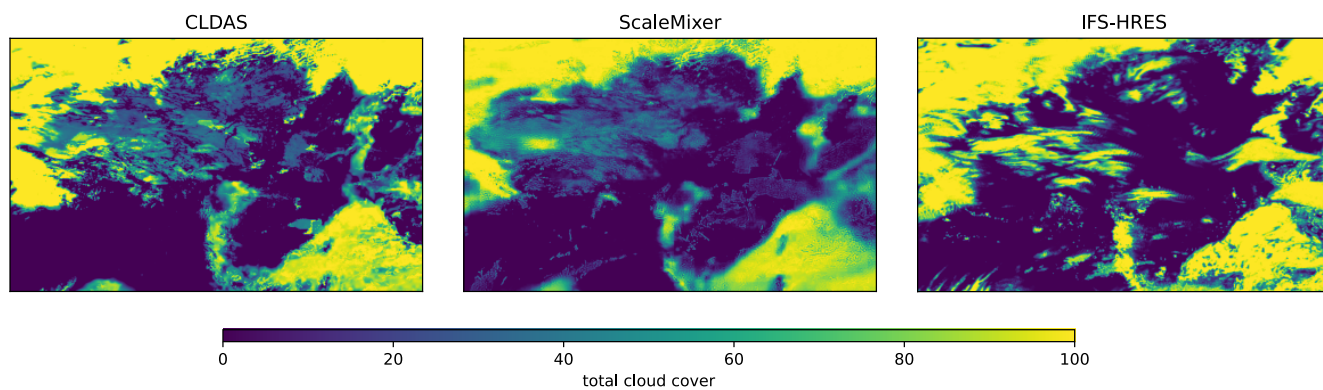
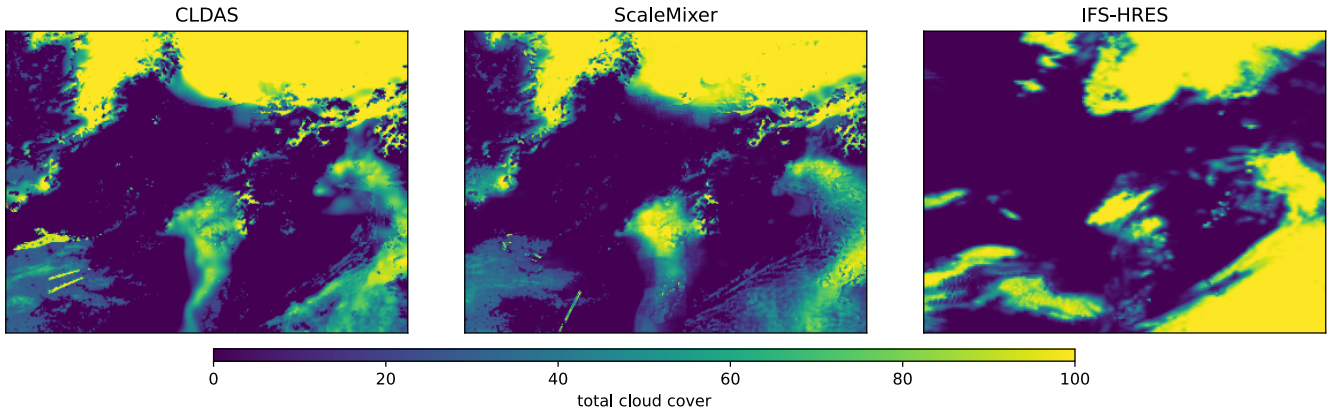


Figure 15: total cloud cover forecasts over China

2025/01/18 13 UTC (Forecast lead time = 1)



2025/01/18 20 UTC (Forecast lead time = 8)

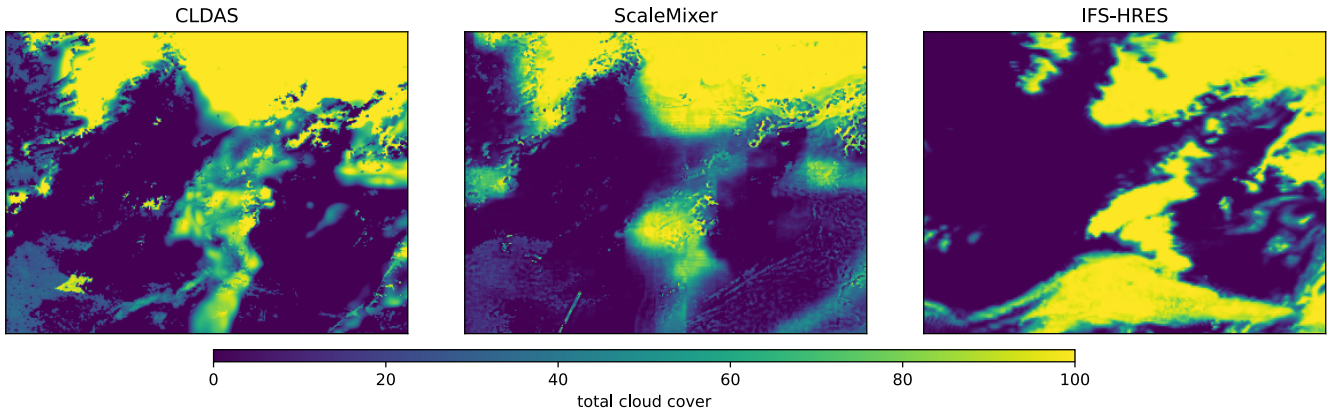


Figure 16: total cloud cover forecasts over a subregion of latitudes in [35, 50] and longitudes in [115, 135]

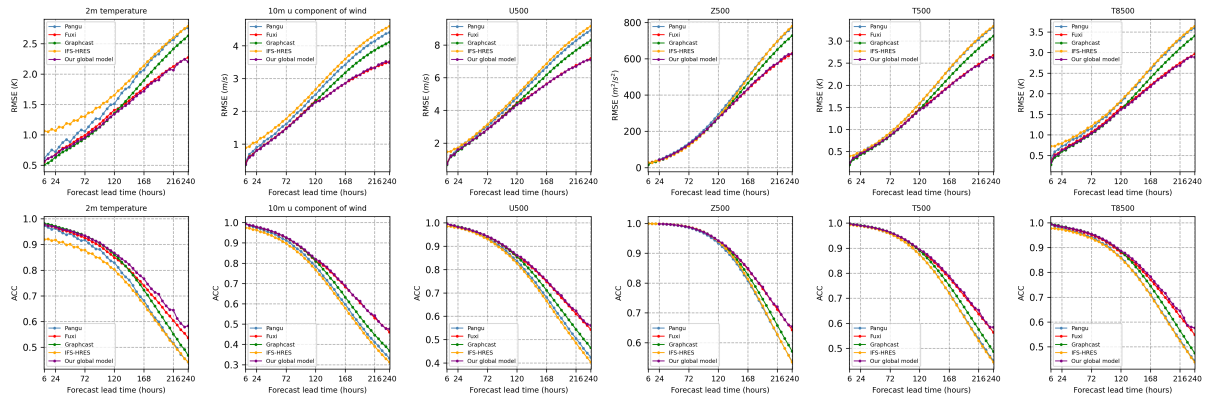


Figure 17: RMSE and ACC for some key variables of various AI-based weather models on Weatherbench2